Journal Pre-proofs

Bio-inspired, sustainable and mechanically robust graphene oxide-based hybrid networks for efficient fire protection and warning

Cheng-Fei Cao, Bin Yu, Bi-Fan Guo, Wan-Jun Hu, Feng-Na Sun, Zhao-Hui Zhang, Shi-Neng Li, Wei Wu, Long-Cheng Tang, Pingan Song, Hao Wang

PII: S1385-8947(22)00024-9
DOI: https://doi.org/10.1016/j.cej.2022.134516
Reference: CEJ 134516

To appear in: *Chemical Engineering Journal*

Received Date: 14 October 2021
Revised Date: 7 November 2021
Accepted Date: 2 January 2022

Please cite this article as: C-F. Cao, B. Yu, B-F. Guo, W-J. Hu, F-N. Sun, Z-H. Zhang, S-N. Li, W. Wu, L-C. Tang, P. Song, H. Wang, Bio-inspired, sustainable and mechanically robust graphene oxide-based hybrid networks for efficient fire protection and warning, *Chemical Engineering Journal* (2022), doi: https://doi.org/10.1016/j.cej.2022.134516

Bio-inspired, sustainable and mechanically robust graphene oxide-based hybrid networks for efficient fire protection and warning

Cheng-Fei Cao, [a] Bin Yu, [*b] Bi-Fan Guo, [c] Wan-Jun Hu, [c] Feng-Na Sun, [c] Zhao-Hui Zhang, [c] Shi-Neng Li, [d] Wei Wu, [e] Long-Cheng Tang, [c] Pingan Song, [a] and Hao Wang [*a]

[a] *Centre for Future Materials, University of Southern Queensland, Springfield Central, 4300, Australia*

[b] *State Key Laboratory of Fire Science, University of Science and Technology of China, Hefei, 230026, PR China*

[c] *College of Material, Chemistry and Chemical Engineering, Key Laboratory of Organosilicon Chemistry and Material Technology, Ministry of Education, Hangzhou Normal University, Hangzhou, 311121, PR China*

[d] *College of Chemistry and Materials Engineering, Zhejiang A & F University, Hangzhou, 311300, PR China*

[e] *Guangdong Provincial Key Laboratory of Technique and Equipment for Macromolecular Advanced Manufacturing, School of Mechanical and Automotive Engineering, South China University of Technology, Guangzhou, 510640, PR China*

[*]Corresponding authors.

E-mail addresses: yubin@ustc.edu.cn (B. Yu), Hao.Wang@usq.edu.au (H. Wang)

Abstract: Effective utilization of natural biomass-derivatives for developing sustainable, mechanically robust, and fireproof materials remains a huge challenge in fire safety and prevention field. Herein, based on bionic design, the hybrid interconnected networks composed of two-dimensional (2D) graphene oxide (GO) nanosheets, renewable one-dimensional (1D) phosphorylated-cellulose nanofibrils (P-CNFs) and tannic acid molecules (TA) were prepared via a green and facile evaporation-induced self-assembly strategy. Through construction of the multiple synergistic interactions among the TA, P-CNFs and GO, the optimized 1D/2D interconnected networks with hierarchical nacre-like structure were achieved and exhibited improved mechanical properties (tensile strength and Young's modulus up to ~132 MPa and ~7 GPa, i.e. ~3.6 and ~14 times higher than that of the pure GO paper), good structural stability in various environments (aqueous solutions with different pH values), excellent flame retardancy (keeping structural integrity after flame attack), and ultrasensitive fire alarm functions (e.g., ultrafast flame alarm time of <1 s and sensitive fire warning responses). Further, such 1D/2D interconnected networks can act as effective flame-retardant nanocoatings to significantly improve the flame retardancy of combustible PU foam materials (e.g., ~48% decrease in peak heat release rate at only 10 wt.% content). Based on the structure observation and analysis, the related synergistic reinforcing and flame-retardant mechanisms were proposed and clarified. Clearly, this work provides a new route for design and development of environmentally friendly fireproof and fire alarm materials based on utilization of natural biomass-derivatives.

Keywords: *Graphene oxide; Biomass-derivatives; Bionic design; Fire protection; Fire early warning*

1. Introduction

The development of human history is accompanied by the acquaintance, control and utilization of fire. Thus, it's probably fair to say that fire plays a crucial role in the progress of human civilization [1]. However, once fire is out of control, it may induce serious fire disasters and lead to a huge loss of life and property. In fact, fire accident is one of the most frequent disasters around the world, which poses significant threatens to the human life, society and environment [2]. For instance, London's Grenfell Tower fire occurred on June 14, 2017, leading to 79 people deaths. Besides, Brazil's National Museum and Notre Dame Cathedral fire accidents in 2018 and 2019 resulted in serious damages of countless item collections and the ancient historical monument. Furthermore, massive forest wildfires that last for months in South Australia had burned at least 17.6 million hectares of land and killed more than 3 billion wildlife lives, which have greatly affected ecological balance [3, 4]. Thus, it is a great global challenge for human to reduce or avoid the occurrence of fire accidents effectively.

To reduce the fire risks, two effective strategies including flame-retardant technologies and fire alarm systems have been explored and developed. The widespread use of flammable materials e.g., natural wood and synthetic polymer is one of main causes of frequent fire accidents. Based on this, a series of flame-retardant technologies such as modification of polymer [5, 6], addition of flame -retardant fillers [7-13] and surface coating [14-17] have been adopted for improving flame retardancy of various combustible materials. The other key strategy is the application of fire alarm sensors or detectors systems for early warning of potential fire hazards. The existing conventional fire alarm detectors mainly include infrared and smoke detectors. Unsatisfyingly, due to the limitation of fire alarm mechanisms, they cannot trigger alarm signals timely before the heat radiation and smoke concentration reached corresponding critical value, thus lead to their long fire alarm responsive time (>100 s) [18, 19]. Besides, poor weather-resistance performance further limits their practical outdoor application. Recently, a series of emerging

fire warning sensors were designed and developed based on various other fire alarm mechanisms. Tang et al first reported a hierarchical graphene oxide (GO)/silicone coating on combustible substrates by dip-coating process [20]. Once encountered flame attack, the silicone resin can provide excellent flame retardancy, GO sheets can be transformed rapidly from insulating state to conductive one and alarm signal can be triggered within 2-3 seconds. Following this work, other research works of GO-based fire alarm sensors were widely investigated and reported recently [21-28]. Meanwhile, other fire alarm sensor systems were also gradually explored based on various alarm mechanisms or sensor materials (e.g., bioinspired color changing molecule, MWCNTs, metallic oxide and MXene, etc.) [29-35], showing promising application in reducing or even avoiding high fire risks of different combustible materials.

Among above fire alarm sensor systems, GO-based fire early detection and warning sensors have been gained most concerns due to their rapid flame alarm response and good designability. However, to obtain desirable fire alarm sensor materials, the introduction of flame-retardant fillers or molecules is needed due to poor flame retardancy and thermal stability of GO sheets. This may involve the use of organic solvents and hazardous chemicals, complicated processing, and high additive contents of fillers. Moreover, considering the rapid flame spreading speed in real fire accidents [36, 37], it is essential to achieve ultrasensitive and reliable fire alarm or abnormal high temperature warning responses in practical application as it can provide people with enough time to handle the potential fires or evacuate. Based on above issues, it is more meaningful to design and develop environmentally friendly flame retardant early fire-warning sensor materials that can provide ultrasensitive and reliable fire alarm responses.

Cellulose is one of the most abundant biopolymers in nature and is widely applied in many fields due to its attractive merits e.g., being sustainable, biodegradable and low cost [38]. Among the many

different types of cellulose, the cellulose nanofibrils (CNFs) with exceptional aspect ratio, good mechanical properties as well as favorable water dispersibility has drawn great attention [39]. However, undesirable high flammability restricts their practical application. Recently, a series of research works of phosphorylated cellulose nanofibrils (P-CNFs) were reported, and the resultant P-CNFs materials prepared after a phosphorylation treatment process show exceptional mechanical and flame-retardant performance [40, 41]. Further, inspired by the layered micro-nano scale structure and multiple interactions of natural nacre, a mechanically robust and flame-retardant GO-based fire alarm sensor material is expected to achieve by introducing P-CNFs into GO network. In addition, for promoting the reduction of GO sheets and thus obtaining sensitive fire alarm response, tannic acid (TA), a typical bio-based polyphenol extracted from plants e.g., oaks, nutgalls and grapes, can be employed as a green and ideal alternative reducing agent [42] since it could be simultaneously used as a reducer and stabilizer for GO sheets [43, 44]. Besides, TA also has the capabilities of radical scavenging effect as well as promoting char-forming [45, 46]. Furthermore, considerable hydroxyl groups of TA structure would provide sufficient possibility for regulating interfacial interactions in GO/TA/P-CNFs hybrid networks. Thus, TA as a multifunctional molecule is expected to improve and balance the comprehensive performance of GO/TA/P-CNFs nanocomposites.

Based on the above design concepts, herein we employ two functional biomass-derivatives i.e., phosphorylated-cellulose nanofibrils (P-CNFs) and tannic acid (TA) to optimize the GO network via evaporation-induced self-assembly strategy (EISA). The presence of P-CNFs significantly improved the flame resistance and mechanical strength of the GO-based hybrid network, and the TA molecules were demonstrated to simultaneously adjust the cross-linking sites in GO/TA/P-CNFs hybrid networks and promote the thermal reduction of GO sheets at high temperatures, thus achieving desirable ultrasensitive fire early warning response. The optimized GO/TA/P-CNFs hybrid networks not only provided an

ultrafast fire alarm time and reliable fire early warning response in precombustion, but showed excellent features e.g., low cost, facile processability, and sustainability. Moreover, the related mechanisms about improved mechanical and flame-retardant performance and fire early warning response were discussed.

2. Experimental

2.1 Materials

Bamboo pulp sheets (bamboo with cellulose content of 96 wt.%) were provided by Hangzhou Bamfox Bamboo Products Co., Ltd. China. Graphite powder was purchased by Shanghai Yifan graphite Co., Ltd. (China). Commercial polyurethane (PU) foam with a density of ~27 kg/m^3 was bought from Zhejiang Hangzhou Guangsheng Foam Plastic Company, China. Tannic acid (TA) was supplied from Beijing Bailingwei Technology Co., Ltd. China. Other chemicals and reagents including potassium permanganate ($KMnO_4$), diammonium hydrogen phosphate ($(NH_4)_2HPO_4$), urea, concentrated sulfuric acid (H_2SO_4, $\geqslant$98 wt%) and hydrogen peroxide (H_2O_2, 30 vol%), were supplied from Sinopharm Chemical Reagent Co., Ltd., China.

2.2 Preparation of GO, P-CNFs and GTP nanocomposite papers

Graphene oxide (GO) sheets were synthesized by using a modified Hummers method via oxidation of natural graphite platelets according to our previous works [47, 48]. Phosphorylated-cellulose nanofibrils (P-CNFs) were synthesized after a phosphorylation treatment process of bamboo pulp sheets, which was introduced in previously reported work [41]. The detailed EISA preparation procedure of GTP (GO/TA/P-CNFs) nanocomposite papers is introduced as follows. Firstly, a certain amount of TA powers was dispersed into the GO solution (4 mg mL^{-1}), and the uniform aqueous GO/TA solution was obtained after a 120 min magnetic stirring process. Next, P-CNFs solution and GO/TA solution were mixed with continuous stirring. Afterward, the resulting mixture suspension was transferred to the mold container and placed in oven at 45 °C for about 16 h. After a slow evaporation process, the GTP

nanocomposite papers were fabricated. For convenience, the GO/TA/P-CNF paper was symbolized as GTP(x/y/z) paper, where x/y/z represents the mass ratio of the various components. For example, $G_1T_{0.5}P_1$ represents the nanocomposite paper containing 1 phr GO, 0.5 phr TA and 1 phr P-CNF, respectively.

2.3 Preparation of PU materials coated with GTP nanocoating

PU materials coated with GTP nanocoating by a simple dip-coating procedure. Briefly, commercial PU foams were washed with ethanol and dried at 80 °C for 2h. Then the PU foams were directly dipped into the as-prepared GO/TA/P-CNFs (1/0.5/1) suspension for 10 min with the assistance of vacuum pump. After that, the samples were placed in an oven and then dried at 80 °C for 6-8 h to obtain the resulting PU foam materials coated with GTP nanocoating. The above procedure was repeated with dip times until the desired content of GTP nanocoating was achieved.

2.4 Characterizations

Fourier transform infrared spectra (FTIR) of various materials and the GTP nanocomposites were carried out on a FTIR spectroscopy (Antaris, Nicolet 7000) in the range of 600 to 4000 cm^{-1}. X-ray photoelectron spectroscopy (XPS) was used to identify the elemental compositions with a photoelectron spectrometer (VG Scientific ESCALab 220I-XL). The morphologies of the samples were characterized by scanning electron microscopy (SEM) (Sigma-500, ZEISS). Transmission electron microscopy (TEM) images were recorded using a high-resolution transmission electron microscope (Tecnai G2 F20S-TWIN) equipped with a field emission gun operating at 200 kV. The tensile properties of GTP paper samples (size: 20 mm in length and 5 mm in width) and compressive characteristics of PU materials samples (size: 20 mm ×20 mm ×10 mm) were tested by a DMA (TA-Q800) at strain rate of 100 (for paper materials) and 2000 $\mu m \cdot min^{-1}$ (for foam materials), respectively. The thermal properties of the samples were performed using thermogravimetric analysis (TGA) (TA Instruments Q500), and the paper samples

were scanned from 35 to 700 °C with a heating rate of 10 °C/min under N_2 atmosphere. The LOI values of PU composites coated GTP coatings were measured using a JF-3 type oxygen index meter in accordance with ASTM Standard D2863-2009 (size: 100 mm ×10 mm ×10 mm). The combustion behaviors of the samples (100 mm×100 mm×10 mm) were carried out by a cone calorimeter device (Fire Testing Technology, UK) according to ISO Method 5660 under a heat flux of 35 kW/m^2. X-ray diffraction (XRD) analysis was recorded on a D/Max 2550 V X-ray diffractor (Rigaku, Japan), and the diffraction patterns were recorded in the 2θ range from 5° to 60° with a scan rate of 5°/min. Electrical resistance transition behaviors of the various paper samples were recorded via connecting a multimeter (ESCORT 3146A) used typical two electrode method. Fire warning performance of paper samples (6 mm width and 20 mm length) was based on self-established alarm system via connecting with wires, an alarm lamp, and a low voltage power supply (~24V).

3. Results and Discussion

3.1 Fabrication and structural characterizations of GTP nanocomposites

Fig. 1a illustrates the schematic fabrication of the GTP paper via a facile EISA strategy. Graphene oxide sheets, tannic acid and phosphorylated-cellulose nanofibrils water solutions were simply mixed to form a homogeneous hybrid solution under magnetic stirring. After low-temperature evaporation process, the ternary nanocomposites of GO/TA/P-CNFs were obtained. **Fig. 1d** and **1e** show the TEM image of 1D phosphorylated-cellulose nanofibrils and the SEM image of 2D graphene oxide sheets, respectively. As expected, P-CNFs exhibits fibrillar morphology with 5-10 nm in diameter and GO shows large planar size with 10-15 μm (**Fig. S1**), which is consistent with the previous results [49, 50]. As we all know, abundant oxygen-containing functional groups including hydroxyl, carboxyl and epoxy groups are existed on the GO sheets surface [51], besides, P-CNFs and TA also have hydroxy or multi-

catechol groups in their molecular structure, thus leading to their good water dispersibility (see **Fig. 1c** and **Fig. S2b**). Consequently, the multiple interactions can be formed among GO nanosheets, P-CNFs and TA molecules, as shown in **Fig. 1b**. On the other hand, the existence of π-π stacking interactions between TA and GO, which is expected to lead to TA molecules further interact with adjacent GO sheets and promote the stacking of GO sheets [52]. Considering the formation of multi-interfacial interaction in GO/TA/P-CNFs hybrid network, Thus, it is reasonable to induce the improvement of resultant nanocomposites in mechanical performance (discussed later).

XPS and FTIR analyses were used to confirm chemical composition and functional groups of three various components. **Fig. 1f** shows XPS results of GO, TA and P-CNFs, two characteristic peaks at C1s (~285.0 eV) and O1s (~533.0 eV) can be clearly observed, and the C/O ratios are quite different i.e., ~2.5 for GO, ~2.1 for TA and ~2.0 for P-CNFs, respectively. It is worth noting that the characteristic peak at P2p (~135.0 eV) can be also found, indicating the successful phosphorylation of bamboo cellulose. The FTIR characteristic peak at 1050 cm^{-1} for the vibration of the epoxy groups (C-O-C) and a broad absorption peak at ~3320 cm^{-1} for the hydroxyl groups (-OH) can be observed for GO sheets [50] (**Fig. 1g**). In addition, it can be also found that the typical peaks at 1620 and 1720 cm^{-1}, which are assigned to the C=C aromatic ring and C=O stretching vibration [53], respectively. The characteristic peaks of TA e.g., 1700 cm^{-1} (C=O stretching), ~1570 cm^{-1} (aromatic ring C=C stretching) and ~1200 cm^{-1} (phenolic C-O stretching) are shown in **Fig. S2a**. Moreover, compared to pristine bamboo bump sheets, the appearance of new peaks at 832, 930 and 1230 cm^{-1} that are responding for the P-O-C, P-OH and P=O (**Fig. S3**), respectively, further demonstrating the successful phosphorylation of cellulose [41]. Above characteristic peaks of P-CNFs and TA can be also found in FTIR spectra of binary GO/P-CNFs and ternary GO/TA/P-CNFs nanocomposite papers, respectively (Fig. 1g).

The multiple interfacial interactions in GO/TA/P-CNFs hybrid network were confirmed by FTIR, Raman spectroscopy, XPS, and XRD analyses. First, after the P-CNF and TA were added into GO, some changes in the peaks of FTIR spectra took place in the composite papers. The peak at ~3320 cm^{-1} attributed to the hydroxyl group (-OH) of GO shifted to the higher wavenumbers (~3340 cm^{-1}) or even weakened (Fig. 1g). Meanwhile, the peak of epoxy group (C-O-C, 1050 cm^{-1}) of GO/TA/P-CNFs showed the gradually decreased intensities with increasing TA content (**Fig. S4**). The red-shift of the peaks of epoxy groups, as well as the decreased intensities of the peak of epoxy group, is usually considered as the evidence of hydrogen bonding [54]. Besides, Raman spectra shows that the presence of P-CNFs and TA makes D band (1346 cm^{-1}) for pure GO paper shift to higher wavenumbers (~1350 cm^{-1}), as shown in **Fig. S5**, indicating the existence of H-bonding. Moreover, the I_D/I_G ratio value decreases from 1.28 for GO to 1.16 for GO/TA/P-CNFs, mainly because of the strong π-π stacking interactions between GO nanosheets and TA molecules [55]. In order to better understanding the existence of multiple interactions, the change of GO/TA/P-CNFs solution after stranded for one week was recorded and compared, as shown in **Fig. 1h**, compared to original GO/TA/P-CNFs hybrid solution (~6 mg mL^{-1}), the obvious increase of viscosity of hybrid solution further demonstrates the existence of multiple interactions between GO, TA, and P-CNFs, in fact, similar phenomenon i.e., the change in rheological behavior of hybrid solutions induced by multiple interactions , was also reported in other previous reported work [54]. Apart from above analyses, XPS and XRD analysis can provide additional evidences to confirm the multiple interactions. Compared to C1s spectrum of pure GO paper (**Fig. S6**), a new peak at 286.1 eV belonging to the binding energy of C-O-P bonds appears in the C1s spectrum of GTP paper, as shown in **Fig. 2f**, indicating that P-CNFs was introduced into the GO interlayer. Furthermore, the peaks of C−O, C=O and C(=O)-O groups in the GTP paper shift from 286.2, 286.9 and 288.5 eV to 286.5, 287.1 and 287.7 eV, respectively, further demonstrating the existence of multiple

interactions i.e., H-bonding and π-π stacking between GO sheets, TA and P-CNFs. XRD results of pure GO paper and GTP nanocomposite papers are shown in **Fig. 2g**. Compared with the sharp diffraction peak of pure GO paper at ~10.94° (interlayer spacing of ~0.87 nm), the G_1P_1 paper shows a large interlayer spacing of ~0.92 nm at ~9.64° with the presence of P-CNFs, indicating the P-CNFs among to the GO sheets [56]. In addition, it is worth noting that TA molecules can further increase the interlayer spacing of GO sheets, more specifically, ~9.30° (~0.95 nm) for $G_1T_{0.1}P_1$, ~8.78° (~1.01 nm) for $G_1T_{0.3}P_1$, respectively. The interlayer spacing increases of GTP nanocomposite papers with increasing the TA contents are attributed to the effective TA intercalation and the formation of multi-interfacial interactions including hydrogen bonding and π-π stacking interactions between GO sheets and TA molecules [43].

As shown in **Fig. 2a**, the as-prepared GTP nanocomposite paper can be bent about 180° without structural fracture, showing good mechanical flexibility. More importantly, due to information of multiple interactions between GO, TA and P-CNFs, the GTP nanocomposite paper exhibits improved strength when compared with pure GO paper (see **Movie S1-S2**). Surface and cross-sectional SEM images of GTP paper present smooth surface and compact microstructure shown in **Fig. 2b** and **2c**, respectively. Besides, after further careful observation, the GTP paper with typical highly aligned structure can be clearly observed in **Fig. 2d**. As mentioned above, the uniform hybrid network of GO/TA/P-CNFs can be formed based on homogenous GO/TA/P-CNFs aqueous solution due to their good water dispersion and multi-interfacial interactions. Cross sectional EDS-mapping images of GTP paper were well confirmed this (see **Fig. 2e**), the appearance and distribution of P element demonstrate the formation of uniform GTP hybrid network. As a result, the GTP nanocomposite paper displays excellent structural stability in harsh conditions even after immersing into strong acid, DI water and alkaline solution as well as organic solvents as shown in **Fig. 2h**, further demonstrating the formation of well cross-linked GO/TA/P-CNFs network structure based on multiple interfacial interactions.

3.2 Mechanical properties and mechanism analysis

The mechanical properties of various nanocomposite papers were investigated and the related results are shown in **Fig. 3a-3c** and **Table S1**. For the binary G_1P_1 paper, it can be clearly seen from the stress-train curves (Fig 3a) that the incorporation of P-CNFs increases the elongation at break as compared to pure GO paper, while this value is lower than P-CNFs paper (**Fig. S7**). The P-CNFs, which is in nanoscale and with high aspect ratio, can form compact interconnected network (**Fig. S8**), and the flexible P-CNFs polymer chain can provide stretchability, thus resulting in its desirable elongation at break. Thus, the elongation at break of G_1P_1 paper can be effectively increased by introducing the P-CNFs. Besides, both of tensile strength and Young's modulus were significantly improved e.g., ~108% and ~180% increase, respectively (Fig 3b and 3c). The above improvements indicate that the effective interface interactions between GO sheets and P-CNFs. For ternary GTP papers, the presence of TA molecules produces further improvement in the tensile strength and the values are strongly dependent on the TA content. More specifically, ~87 MPa for $G_1T_{0.1}P_1$ paper, ~102 MPa for $G_1T_{0.3}P_1$ paper and ~132 MPa for $G_1T_{0.5}P_1$ paper, respectively, compared to pure GO paper of ~36.7 MPa. Moreover, similar obvious improvement in Young's modulus can be also found in Fig 3c and Table S1. Interestingly, along with the increases in tensile strength, the elongation at break of GTP papers was gradually decreased with increasing TA content. It is worth noting that with a higher content of TA, the GTP paper shows obvious brittleness, and crack is observed in resultant $G_1T_{0.7}P_1$ paper sample (**Fig. S9**). Summarizing and analyzing above results, it is clear that the synergistic reinforcing effect based on multiple interfacial interactions was formed in GO/TA/P-CNFs hybrid network.

In order to unveil the reinforcing mechanism of TA-P-CNFs in GO network, the cross-sectional morphology of various paper nanocomposites after tests were characterized by SEM and shown in **Fig. 4a-4c**. Pristine GO paper presented a smooth fracture edge (see Fig. 4a), which is consistent with

previously reported results [57-59]. In comparison, the presence of P-CNFs leads to rough fracture edge and slightly loose hierarchical structure (Fig. 4b). With further observation, many fibrils can be easily found on the edge of broken GO sheets, in fact, such fibril-like structure is P-CNFs that intercalated to GO network. Interestingly, $G_1T_{0.5}P_1$ paper sample displays a relatively compact and aligned structure when compared with G_1P_1 paper (see Fig. 4c). Notably, a visible saw-like structure appeared on the edge of integrated GO/TA/P-CNFs network, which was induced by the presence of TA molecules. Based on the analysis of fracture morphologies of various samples, the crack extension model is proposed, as shown in **Fig. 4d**. For pure GO paper, due to weak bonding between the GO sheets, immediate fracture will occur after being stretching, thus produce smooth fracture edge. Comparatively, for GO/TA/P-CNFs hybrid network, due to the existence of abundant hydroxyl groups in TA and P-CNFs structure, multiple interactions e.g., hydrogen bonds and π-π stacking can further strengthen cross-linking network of GO/TA/P-CNFs nanocomposites. When the GO/TA/P-CNFs ternary nanocomposites are subjected to stretch, the hydrogen bond interactions in GO/TA/P-CNFs network are first destroyed, and the GO sheets begin to slide over each other and the crack appears [60]. However, the flexible P-CNFs polymer chains can bridge the crack and restrict the further crack growth of GO sheets. With continuous stretching, the P-CNFs that attached to GO sheets start to slide and move. Subsequently, partial P-CNFs chain are damaged and pulled out and remaining unbroken chains still bridge GO sheets. This process would continue before the GO/TA/P-CNFs ternary nanocomposites complete fracture， which resulting the saw-like edge shown in Fig. 4c. Therefore, much more energy is absorbed during whole process, thus induce higher strength. Additionally, the introduction of the TA is responsible for the increase in tensile strength and Young's modulus and the decrease in tensile strain (Fig. 3). Due to the presence of TA molecules, cross-linking sites of GO/TA/P-CNFs hybrid network have increased via multiple hydrogen bonding interactions, which likely induces the confinement in movement of the polymer chain, thus

leading to the increase in stiffness values and the decrease in breaking extension of the nanocomposites. This can explain the discrepancy of fracture morphology and mechanical properties of binary G_1P_1 and ternary $G_1T_{0.5}P_1$ samples.

3.3 Flame-retardant performance and thermal stability

To evaluate the effect of introduction of TA and P-CNFs on the flame retardancy of GO paper, the flame burning tests were conducted and the related whole combustion process of pure GO and GO nanocomposite papers can be obtained from **Movie S3**. As shown in **Fig. 5a–5c**, paper samples were directly exposed to ethanol flame with a temperature of 500-600 °C. As expected, due to abundant of unstable oxygen groups e.g., hydroxyl, epoxy and carboxyl groups on GO sheets surface, the pure GO paper displays drastic combustion and rapid decomposition behavior once being ignited and can be completely burned off within only ~ 90 s, which is well consistent with previous reports [50, 57]. Comparatively, $G_1T_{0.5}$ paper shows improved flame resistance, which was due to charring and radical quenching effects of TA with phenolic structure [45, 46, 61]. However, it still can be gradually decomposed under continuous flame attack condition. Satisfyingly, the $G_1T_{0.5}P_1$ paper exhibits excellent flame retardancy, only a little shrinkage can be observed after being burned, which was quite different compared with the pure P-CNFs paper (see **Fig. S10**). Besides, its structural integrity still be maintained and shape and size are almost unchanged during whole combustion process, demonstrating the presence of P-CNFs was greatly enhanced the flame resistance of GO paper. **Fig. 5d** shows the FTIR results of the GTP paper before and after burning test. The disappearance of characteristic peaks of oxygen-containing groups indicates thermal degradation of GTP network.

TGA measurements were also conducted and corresponding TGA curves of pure GO, G_1P_1 and $G_1T_{0.5}P_1$ papers are shown in **Fig. 5e**. It is clear that all paper samples started to lose weight below 100 °C, this is due to the volatilization of water molecules stored in their network structure [50]. Besides, the

second obvious weight loss in these composite papers occurred at the stage of 180−220 °C, due to the thermal pyrolysis/decomposition of oxygen-containing groups of their structure and the release of CO_2, CO, and gas. After that, with increasing temperature, the thermal degradation of above nanocomposite papers was processing slowly and smoothly. Comparatively, the $G_1T_{0.5}$ paper exhibited better thermal stability than that of pure GO paper, due to the radical scavenging effect and char-forming capabilities of TA molecule. Moreover, with the presence of P-CNFs, the thermal stability of nanocomposite paper was further improved, which may due to the compact P-CNFs can provide more effective physical barrier effect and stabilized the RGO/TA network. As a result, the final weight of $G_1T_{0.5}P_1$ paper at 750 °C is more than that of pure GO paper and $G_1T_{0.5}$ paper e.g., 50.8% for $G_1T_{0.5}P_1$ paper, 47.7% for $G_1T_{0.5}$ paper and 38.7% for GO paper, respectively. TGA results of various nanocomposite papers are consistent with their burning behaviors. In order to visually exhibit the difference of paper materials in thermal stability, the pure GO paper and GTP nanocomposite paper were treated under high temperature environmental condition (300 °C) for 30 min. As shown in **Fig. 5f**, pure GO paper presents obvious structural damage and the decomposition products, in the form of black ash, were clearly visible on the edge of rGO paper. By comparison, the $G_1T_{0.5}P_1$ paper shows good structural integrity, after high temperature treatment, the $G_1T_{0.5}P_1$ paper still maintained its initial shape and irregular edge can be also observed, except for a bit of shrinkage, further demonstrating the excellent thermal stability of GO/TA/P-CNFs network.

3.4 Analysis of flame-retardant mechanism

To ascertain the flame-retardant mechanisms, the surface and cross-sectional morphology of GO and $G_1T_{0.5}P_1$ paper after the burning test was imaged and compared as shown in **Fig. 6a** and **6b**. For burned pure GO paper, loose structure can be easily observed (Fig. 6a-i) and many obvious microcracks appeared on its surface zone (Fig. 6a-ii), which were due to the breakage of surface char protective layer

[58]. The existence of many microcracks has obvious effect on the flame retardancy and thermal stability of GO network, as these microcracks hardly restrict the heat and oxygen to attack the inside GO network, thus inducing the structural damage of GO paper. In comparison, smooth and compact protective char layer is clearly observed on the surface of $G_1T_{0.5}P_1$ paper after burned (Fig. 6b-i), with further observation, some nanoparticles appeared on its surface protective layer (Fig. 6b-ii). The SEM images of cross-section morphology can be offered more evidences. Compared to highly aligned and dense structure of pristine $G_1T_{0.5}P_1$ paper before burned (Fig. 2d), the loose layered microstructure after burned can clearly observe, and the rGO sheets are stacked together (Fig. 6b-iii). In addition, the spacing between rGO sheets has increased greatly, which was due to the release of decomposition products e.g., H_2O, CO_2 and other gas from three various components during combustion process [62]. Interestingly, similar phenomenon was observed in rGO sheets surface. The high-magnification SEM image in Fig. 6b-iv discloses that many nanoparticles with the size of 50-200 nm were also attached on rGO sheets, which may be phosphorus-oxygen compounds generated by P-CNFs after burning test [41]. The XPS survey results can well demonstrate above interpretation (**Fig. 6c-6e**). Firstly, there is an obvious change of C/O ratio from 2.2 to 6.3 after burned (see Fig. 6c), besides, the percentage of the binding energy of oxygen-containing groups i.e., C–O, C=O and C (=O) O also has decreased shown in C1s core level spectra (Fig. 6d), indicating the thermal decomposition process of $G_1T_{0.5}P_1$ paper. Moreover, the characteristic peaks of phosphorus-containing structure (**Fig. 6e**) and SEM-EDS mapping (**Fig. S11**) further implied the formation of PxOy compound due to thermal transformation of phosphorus-containing group of P-CNFs during burning process [41].

Based on the structural analysis and related XPS results, the proposed flame-retardant mechanism is illustrated in **Fig. 6f**. Normally, the loose and porous architecture was formed from ordered and dense one due to the gases release from thermal degradation of abundant oxygen-containing groups. On the

one hand, the TA molecule with multi-catechol groups can act as a radical scavenger, along with its charring capacity [45, 61], thus lead to the enhanced flame retardancy of GO paper (see Fig. 6b). On the other hand, nano-size fibrillar P-CNFs can further stabilize the hybrid char layer effectively during the combustion process, which is the main factor of the formation of compact protective layer. As a result, the external oxygen attack and thermal degradation of internal GO/TA/P-CNFs hybrid network were restricted efficiently due to the compact physical barrier effect. For P-CNFs, the thermal decomposition and dehydration processes of its phosphorus-containing groups induced the gases release e.g., H_2O and CO/CO_2, which can dilute the concentration of oxygen. Besides, the decomposition product P_xO_y compound, in the form of nano-particles, was well re-deposited on rGO sheets and further inhibit the thermal decomposition of rGO sheets due to its free radical catching effect, resulting in the improved flame retardancy of GTP nanocomposites.

3.5 Response performance of fire early warning

Owing to its excellent mechanical properties and ideal flame retardancy, such GTP hybrid network can be used as ideal fire alarm sensor material. **Fig. 7c** presents the schematic illustration of construction and working mechanism of fire warning system based on the thermal-induced resistance transition of GO (**Fig. 7d**). The paper sample (20 mm length and 6 mm width) was connected with an alarm lamp and a low-voltage electric source (~24V) through wires, and the fire alarm system was established. Upon encounter the flame or high temperature environments, the GO sheets will be thermally reduced and an electrically conductive path can be formed [20], thus lead to trigger the alarm lamp. To evaluate the practical fire alarm response behaviors, the different paper samples were selected and corresponding comparative studies were conducted. The flame detection and warning process of various paper samples are shown in **Fig. 7a** and **7b**, **Fig. S12** and **Movie S4**. When placed in the ethanol flame, the GO paper was quickly burned out within 10 s due to its poor flame retardancy and structural stability and the alarm

lamp was not triggered (Fig. S12). On the contrary, for the $G_1T_{0.5}$ paper, rapid danger alarm can be released within ~1 s after encountered flame attack, however, the sample was burned out and alarm signal disappeared after 10 s combustion (see Fig. 7a), which means $G_1T_{0.5}$ paper cannot provide continuous alarm signal. Comparatively, when $G_1T_{0.5}P_1$ paper is attacked by the alcohol lamp flame, danger alarm signal can also be sent within 1 s. Meanwhile, the signal can be well maintained after 120 s flame combustion, and continuous alarm was kept even after removing the flame resource. Besides, in order to measure fire alarm response time of samples, the electrical transition behaviors were monitored and alarm line was defined based on electrical decrease (the danger alarm can release after ~four orders of magnitude decrease in electrical resistance). The electrical resistance transition of $G_1T_{0.5}P_1$ paper after encountered flame attack is shown in **Fig. 7e**. It can be clearly seen that rapid electrical transition was triggered and corresponding electrical resistance change of over four orders of magnitude can be completed within 1 s, which is consistent with the fire warning behavior of $G_1T_{0.5}P_1$ paper in practical test. (Fig. 7b).

Considering the quick flame spreading speed in fire accidents [36, 63], the fire warning response before combustible materials ignited is particularly important for reducing or avoiding possible life and property loss. Thus, the high temperature warning response behaviors and corresponding electrical resistance changes of GO and GTP papers under different high temperature conditions were also monitored and compared. The test method and the related high temperature warning processes are shown in **Fig. S13a** and **Movie S5-S6**. In the case of 150 °C, clearly, the electrical resistance of GO paper was almost unchanged during the 300 s treatment process, accordingly, the danger alarm was not triggered (Fig. S12). This is due to the thermal reduction of GO sheets cannot be completed within 300 s [62]. Comparatively, the GTP paper can trigger danger alarm within ~180 s for 150 °C and a faster response of ~45 s can achieve under temperature of 200 °C shown in see **Fig. S10b**， indicating an effective fire

early response performance. In addition, as expected, the GTP paper shows more rapidly electrical resistance transition behaviors with increasing the hot surface temperature (**Fig. 7f**). The detailed high temperature warning response time for GO paper and GTP paper are shown in **Fig. 7g**, it is obvious that, for a fixed temperature, GTP paper exhibits quicker electrical resistance transition and less alarm response time than GO paper e.g., 27 s for 250 °C, 10 s for 300 °C and 3 s for 350 °C, respectively. Besides, it is worth noting that GO paper cannot trigger the alarm lamp and normal resistance change was also unavailable when it was placed in conditions of over 300 °C. GO network would decompose with seconds and further leading to the broken structure under such high temperature environments, thus leading to above results. Previously reported works showed that the temperature-responsive behaviors of GO-based fire alarm sensors are mainly dependent on the thermal reduction process of GO network [26, 64, 65]. The different electrical resistance changing behaviors of GO and GTP papers suggest that the presence of TA molecules can accelerate thermal reduction process of GO sheets at high temperature of 150–350 °C, thus leading to the sensitive electrical resistance transition and efficient abnormal high temperature warning response during the precombustion stage of combustible materials. In fact, the reduction mechanism of GO by TA molecules was first proposed by Guo et al [44]. Following this work, a series of works related to the reduction of GO by TA were demonstrated and reported [42, 66, 67]. Specifically, the mechanism involving the removal of epoxy and hydroxyl based on a two-step $S_N 2$ nucleophilic reactions and an elimination reaction, the relevant detailed reaction processes as shown in **Fig. S15**. Based on above analysis and discussion, it is reasonable to understand the ideal fire alarm response performance of GTP network.

Such fire early warning sensor based on GTP hybrid network is compared to previously reported other different types of fire alarm sensor systems, in terms of fabrication method, sustainability and flame/high temperature alarm response time, and the comparative items and results are shown in **Table**

1. After a comprehensive comparison, it is clear that the as-designed fire-warning sensor is superior to other counterparts. Firstly, compared to other works which involved the use of organic solvents or complicated fabrication process [20, 68-70], the fabrication method of as-designed sensor material is simple and environmentally friendly. Besides, like precious works e.g., SPI/MSF-g-COOH/CA/GN film [71] and SF/Ca^{2+} i-skin [72], the use of biomass materials in this work also shows the sustainability of as-prepared fire alarm sensor material. More importantly, the fire early warning sensor based on GTP network possesses ultrasensitive temperature-responsive function compared to other previous sensor systems with high temperature warning functions [20, 25, 26, 62, 64, 68-70, 73]. Based on above comparison and analysis, as-designed fire alarm sensor shows promising fire warning application.

3.6 Fire safety application of GTP hybrid nanocoating

Polymer foams, represented by polyurethane foam (PUF), have been widely applied in a wide range of fields due to their excellent properties, including inexpensiveness, lightweight, thermal insulation as well as mechanical flexibility [74]. Unfortunately, owing to its intrinsic highly flammability, there are numerous fire accidents occurred caused by PUF around the world each year, and resulting disasters lead to huge life and property losses [75]. Thus, it is urgent to effectively improve fire retardancy of combustible PUF. The abovementioned results and discussions indicate that the GTP networks can be used as a green flame retardant nanocoating apply in PU foam due to its high performance e.g., good mechanical properties, structural stability and excellent flame retardancy. Herein, the surface coating technique was adopted and PU foam materials coated with the hybrid GTP nanocoating were prepared by a simple dip-coating process, and their structure and morphology, mechanical and flame retardancy performance were investigated systematically. **Fig. 8a-8c** show the SEM images of the PU foam coated GTP nanocoating (totaling 30 wt.% coating mass). As presented in Fig. 8a, the GTP coated foam shows a macroscopic porous structure similar to original PU foam and the blocking pore phenomena did not

appear in the PU foam pores. Besides, good adhesion can be formed between the nanocoating and PU matrix as N-H groups of skeleton surfaces can interact with hydroxyl groups of the hybrid GTP network, thus the GTP nanocoating was well wrapped on PU skeleton as shown in Fig. 8b. With higher magnification suggests that the thickness of GTP coating was only about ~300 nm (Fig. 8c). Furthermore, such nanocoating also shows ideal stability in aqueous environments with 30 min bath sonication treatment (**Fig. S16**), which further demonstrates highly compact and interconnected networks of GTP nanocoating. **Fig. 8e** shows the processes of cyclic compression tests of the foam samples. The results show that both PU foam composites display good compressibility and structural stability as their compressive stress values at 60 % strain are almost unchanged even after the ~100 times cyclic compression. Besides, the compressive strength of the PU foam shows obvious improvements after coated GTP nanocoating, normally, the higher content of GTP nanocoating induce much higher value in the maximum compressive stress e.g., ~16.8 kPa for the PU-GTP30% and ~10.0 kPa for the PU-GTP10%, which is superior to that of pure PU foam with ~4.0 kPa. To evaluate the flame-retardant performance of PU foam materials coated GTP nanocoating, flame combustion tests were conducted (see **Fig. 8d**). It shows that the pure PU foam sample was easily ignited followed by fiercely burning with extensive melt drippings, and whole sample was complete combustion within 10 s (see Fig. 8d-i) [14]. For PU-GTP10% sample, although the flame was quickly spread to the entire foam sample, no melt drippings were observed and the original size and structural integrity of foam sample were well maintained even after combustion (Fig. 8d-ii). With a high content of 30 wt.% GTP coatings, there was no flame spreading and the foam sample can be self-extinguishing within 2 s after removing flame resource (Fig. 8d-iv). To demonstrate the above improved flame retardancy, the limiting oxygen index (LOI) values of various samples were measured and shown in **Fig. 8f**. As expected, compared with the low LOI value of ~17.5 for pure PU foam, the PU-GTP10%, PU-GTP20% and PU-GTP30% foam

materials have ~20.0%, ~22.8% and ~24.6%, respectively, which was consistent with above combustion behaviors of various foam samples. Cone calorimetry tests of various foam samples were further conducted and detailed data are shown in **Table. S2**. As expected, the peak heat release rate (pHRR) of pure PU foam is high up to ~318 kW/m^2, with only 10 wt.% GTP nanocoating, it can achieve a 48% decrease in pHRR. Additionally, the nanocoating also produces increased char residual weight, e.g., 25% for PU-GTP10% and 30% for PU-GTP30%, compared with 5% for pure PU foam. Moreover, compared with the complete combustion of the pure PU foam with a little char residue, the char of the PU sample coated GTP nanocoating shows structure integrity and almost unchanged size (**Fig. S17**.). Above results further demonstrate that such hybrid GTP hybrid network can be also used as effective green flame-retardant coating for improving the flame resistance of flammable PU foam materials.

4. Conclusion

In summary, based on bionic design, by well exploring and utilizing the characteristics and functions of two natural biomass-derivatives (i.e., TA and P-CNFs), a sustainable, mechanically robust and flame-retardant GO/TA/P-CNFs hybrid network was designed and prepared via a facile EISA approach. The mechanical properties of the paper nanocomposites were greatly improved due to the successful formation of multi-interactions i.e., H-bonding and π-π stacking in hybrid networks (tensile strength and Young's modulus reach ~132 MPa and ~7 GPa, i.e. ~3.6 and ~14 times higher than that of the pure GO paper, respectively). Besides, GO/TA/P-CNFs hybrid networks exhibited good structural stability in harsh conditions resulting from multiple interactions among the hybrid network and exceptional flame retardancy due to the introduction of TA and P-CNFs. Notably, with the presence of TA, thermal reduction of GO sheets was further promoted in high temperatures, thus the optimized GO/TA/P-CNFs hybrid networks showed ultrafast fire alarm time of <1s and sensitive high temperature warning responses (e.g., 3 s at 350 °C, 27 s at 250 °C and 45 s at 200 °C), which is much more remarkable and

sensitive than previous reported works. Moreover, such hybrid networks can act as flame retardant nanocoatings for improving the flame retardancy of combustible PU foam materials (~48% reduction in the peak heat release rate with only 10 wt.% content). With numerous features e.g., low cost, facile processability, and sustainability, such GO/TA/P-CNFs hybrid networks can be applied as desirable fireproof and fire alarm sensor materials in fire safety and prevention field. Hence, this work not only extends the development of green bio-based fire alarm sensor materials but also provides a new path for exploring the application of bio-mass materials.

Conflicts of interests

There are no conflicts to declare.

Acknowledgements

The research work was supported by the Australian Research Council Training Centre in Fire Retardant Materials and Safety Technologies (IC170100032), Australian Research Council Discovery Early Career Researcher Award (DE190101176) and the International Collaboration Programs of Guangdong Province (2020A0505100010).

References

[1] D.M. Bowman, J.K. Balch, P. Artaxo, W.J. Bond, J.M. Carlson, M.A. Cochrane, C.M. D'Antonio, R.S. Defries, J.C. Doyle, S.P. Harrison, F.H. Johnston, J.E. Keeley, M.A. Krawchuk, C.A. Kull, J.B. Marston, M.A. Moritz, I.C. Prentice, C.I. Roos, A.C. Scott, T.W. Swetnam, G.R. van der Werf, S.J. Pyne, Fire in the Earth system, Science, 324 (2009) 481-484.

[2] J.M. Fox, G.M. Whitesides, Warning signals for eruptive events in spreading fires, Proc Natl Acad Sci U S A, 112 (2015) 2378-2383.

[3] H.I. Jager, C.C. Coutant, Knitting while Australia burns, Nature Climate Change, 10 (2020) 170-170.

[4] D.B. Lindenmayer, R.M. Kooyman, C. Taylor, M. Ward, J.E.M. Watson, Recent Australian wildfires made worse by logging and associated forest management, Nature Ecology & Evolution, 4 (2020) 898-900.

[5] W.T. He, P.A. Song, B. Yu, Z.P. Fang, H. Wang, Flame retardant polymeric nanocomposites through the combination of nanomaterials and conventional flame retardants, Prog Mater Sci, 114 (2020) 100687.

[6] S. Huo, P. Song, B. Yu, S. Ran, V.S. Chevali, L. Liu, Z. Fang, H. Wang, Phosphorus-containing flame retardant epoxy thermosets: Recent advances and future perspectives, Progress in Polymer Science, 114 (2021) 101366.

[7] X. Zhou, S.L. Qiu, X.W. Mu, M.T. Zhou, W. Cai, L. Song, W.Y. Xing, Y. Hu, Polyphosphazenes-based flame retardants: A review, Compos Part B-Eng, 202 (2020) 108397.

[8] H. Yang, B. Yu, X. Xu, S. Bourbigot, H. Wang, P. Song, Lignin-derived bio-based flame retardants toward high-performance sustainable polymeric materials, Green Chemistry, 22 (2020) 2129–2161.

[9] X. Wang, E.N. Kalali, J.-T. Wan, D.-Y. Wang, Carbon-family materials for flame retardant polymeric materials, Progress in Polymer Science, 69 (2017) 22-46.

[10] Y. Shi, C. Liu, Z. Duan, B. Yu, M. Liu, P. Song, Interface engineering of MXene towards super-tough and strong polymer nanocomposites with high ductility and excellent fire safety, Chemical Engineering Journal, 399 (2020) 125829.

[11] B. Yu, W. Xing, W. Guo, S. Qiu, X. Wang, S. Lo, Y. Hu, Thermal exfoliation of hexagonal boron nitride for effective enhancements on thermal stability, flame retardancy and smoke suppression of epoxy resin nanocomposites via sol–gel process, Journal of Materials Chemistry A, 4 (2016) 7330-7340.

[12] B. Yu, B. Tawiah, L.Q. Wang, A.C. Yin Yuen, Z.C. Zhang, L.L. Shen, B. Lin, B. Fei, W. Yang, A. Li, S.E. Zhu, E.Z. Hu, H.D. Lu, G.H. Yeoh, Interface decoration of exfoliated MXene ultra-thin nanosheets for fire and smoke suppressions of thermoplastic polyurethane elastomer, J Hazard Mater, 374 (2019) 110-119.

[13] W. Wu, W. Zhao, X. Gong, Q. Sun, X. Cao, Y. Su, B. Yu, R.K.Y. Li, R.A.L. Vellaisamy, Surface decoration of halloysite nanotubes with POSS for fire-safe thermoplastic polyurethane nanocomposites, Journal of Materials Science & Technology, (2021).

[14] H. Kim, D.W. Kim, V. Vasagar, H. Ha, S. Nazarenko, C.J. Ellison, Polydopamine-Graphene Oxide Flame Retardant Nanocoatings Applied via an Aqueous Liquid Crystalline Scaffold, Advanced Functional Materials, 28 (2018) 1803172.

[15] D. Lin, X. Zeng, H. Li, X. Lai, T. Wu, One-pot fabrication of superhydrophobic and flame-retardant coatings on cotton fabrics via sol-gel reaction, J Colloid Interface Sci, 533 (2019) 198-206.

[16] Y. Li, C.-F. Cao, S.-N. Li, N.-J. Huang, M. Mao, J.-W. Zhang, P.-H. Wang, K.-Y. Guo, L.-X. Gong, G.-D. Zhang, L. Zhao, L.-Z. Guan, Y.-J. Wan, L.-C. Tang, Y.-W. Mai, In situ reactive self-assembly of a graphene oxide nano-coating in polymer foam materials with synergistic fire shielding properties, Journal of Materials Chemistry A, 7 (2019) 27032-27040.

[17] Z. Ma, X. Liu, X. Xu, L. Liu, B. Yu, C. Maluk, G. Huang, H. Wang, P. Song, Bioinspired, Highly Adhesive, Nanostructured Polymeric Coatings for Superhydrophobic Fire-Extinguishing Thermal Insulation Foam, ACS Nano, 15 (2021) 11667−11680.

[18] J.R. Qualey Iii, Fire Test Comparisons of Smoke Detector Response Times, Fire Technol., 36 (2000) 89-108.

[19] D.D. Evans, D.W. Stroup, Methods to calculate the response time of heat and smoke detectors installed below large unobstructed ceilings, Fire Technol., 22 (1986) 54-65.

[20] Q. Wu, L.-X. Gong, Y. Li, C.-F. Cao, L.-C. Tang, L. Wu, L. Zhao, G.-D. Zhang, S.-N. Li, J. Gao, Y. Li, Y.-W. Mai, Efficient Flame Detection and Early Warning Sensors on Combustible Materials Using Hierarchical Graphene Oxide/Silicone Coatings, ACS Nano, 12 (2017) 416-424.

[21] F.F. Chen, Y.J. Zhu, F. Chen, L.Y. Dong, R.L. Yang, Z.C. Xiong, Fire Alarm Wallpaper Based on Fire-Resistant Hydroxyapatite Nanowire Inorganic Paper and Graphene Oxide Thermosensitive Sensor, ACS Nano, 12 (2018) 3159-3171.

[22] H. Xie, X. Lai, H. Li, J. Gao, X. Zeng, X. Huang, X. Lin, A highly efficient flame retardant nacre-inspired nanocoating with ultrasensitive fire-warning and self-healing capabilities, Chemical Engineering Journal, 369 (2019) 8-17.

[23] G. Chen, B. Yuan, Y. Wang, X. Chen, C. Huang, S. Shang, H. Tao, J. Liu, W. Sun, P. Yang, G. Shi, Nacre-biomimetic graphene oxide paper intercalated by phytic acid and its ultrafast fire-alarm application, J Colloid Interface Sci, 578 (2020) 412-421.

[24] W. Liu, X. Wang, Y. Song, R. Cao, L. Wang, Z. Yan, G. Shan, Self-powered forest fire alarm system based on impedance matching effect between triboelectric nanogenerator and thermosensitive sensor, Nano Energy, 73 (2020) 104843.

[25] F. Khan, S. Wang, Z. Ma, A. Ahmed, P. Song, Z. Xu, R. Liu, H. Chi, J. Gu, L.C. Tang, Y. Zhao, A Durable, Flexible, Large-Area, Flame-Retardant, Early Fire Warning Sensor with Built-In Patterned Electrodes, Small Methods, 5 (2021) 2001040.

[26] Z. Qu, C.-a. Xu, X. Li, Y. Wu, K. Wang, X. Zheng, X. Cui, X. Wu, J. Shi, K. Wu, Facile preparation of BP-MoS2/GO composite films with excellent flame retardancy and ultrasensitive response for smart fire alarm, Chemical Engineering Journal, 426 (2021) 130717.

[27] B. Nan, K. Wu, Z. Qu, L. Xiao, C. Xu, J. Shi, M. Lu, A multifunctional thermal management paper based on functionalized graphene oxide nanosheets decorated with nanodiamond, Carbon, 161 (2020) 132-145.

[28] G. Chen, B. Yuan, Y. Zhan, H. Dai, S. He, X. Chen, Functionalized graphene paper with the function of fuse and its flame-triggered self-cutting performance for fire-alarm sensor application, Materials Chemistry and Physics, 252 (2020) 123292.

[29] T. Fu, X. Zhao, L. Chen, W.-S. Wu, Q. Zhao, X.-L. Wang, D.-M. Guo, Y.-Z. Wang, Bioinspired Color Changing Molecular Sensor toward Early Fire Detection Based on Transformation of Phthalonitrile to Phthalocyanine, Advanced Functional Materials, 29 (2019) 1806586.

[30] M. Zhang, M. Wang, M. Zhang, C. Yang, Y. Li, Y. Zhang, J. Hu, G. Wu, Flexible and Thermally Induced Switchable Fire Alarm Fabric Based On Layer-by-Layer Self-Assembled Silver Sheet/Fe_3O_4 Nanowire Composite, ACS Appl Mater Interfaces, 11 (2019) 47456-47467.

[31] J. Chen, H. Xie, X. Lai, H. Li, J. Gao, X. Zeng, An ultrasensitive fire-warning chitosan/montmorillonite/carbon nanotube composite aerogel with high fire-resistance, Chemical Engineering Journal, 399 (2020) 125729.

[32] B. Wang, X. Lai, H. Li, C. Jiang, J. Gao, X. Zeng, Multifunctional MXene/Chitosan-Coated Cotton Fabric for Intelligent Fire Protection, ACS Appl Mater Interfaces, 13 (2021) 23020−23029.

[33] H. Xie, X. Lai, H. Li, J. Gao, X. Zeng, Skin-inspired thermoelectric nanocoating for temperature sensing and fire safety, J Colloid Interface Sci, 602 (2021) 756-766.

[34] Q. Yu, P. Weng, L. Han, X. Yin, Z. Chen, X. Hu, L. Wang, H. Wang, Enhanced thermal conductivity of flexible cotton fabrics coated with reactive MWCNT nanofluid for potential application in thermal conductivity coatings and fire warning, Cellulose, 26 (2019) 7523-7535.

[35] M. Mao, K.-X. Yu, C.-F. Cao, L.-X. Gong, G.-D. Zhang, L. Zhao, P. Song, J.-F. Gao, L.-C. Tang, Facile and green fabrication of flame-retardant Ti3C2Tx MXene networks for ultrafast, reusable and weather-resistant fire warning, Chemical Engineering Journal, 427 (2022) 131615.

[36] E. Guillaume, V. Dréan, B. Girardin, F. Benameur, M. Koohkan, T. Fateh, Reconstruction of Grenfell Tower fire. Part 3—Numerical simulation of the Grenfell Tower disaster: Contribution to the understanding of the fire propagation and behaviour during the vertical fire spread, Fire and Materials, 44 (2019) 35-57.

[37] S.T. McKenna, N. Jones, G. Peck, K. Dickens, W. Pawelec, S. Oradei, S. Harris, A.A. Stec, T.R. Hull, Fire behaviour of modern facade materials - Understanding the Grenfell Tower fire, J Hazard Mater, 368 (2019) 115-123.

[38] E.S. Ferreira, C.A. Rezende, E.D. Cranston, Fundamentals of cellulose lightweight materials: bio-based assemblies with tailored properties, Green Chemistry, 23 (2021) 3542-3568.

[39] H. Qin, Y. Zhang, J. Jiang, L. Wang, M. Song, R. Bi, P. Zhu, F. Jiang, Multifunctional Superelastic Cellulose Nanofibrils Aerogel by Dual Ice-Templating Assembly, Advanced Functional Materials, (2021) 2106269.

[40] M. Ghanadpour, F. Carosio, M.C. Ruda, L. Wagberg, Tuning the Nanoscale Properties of Phosphorylated Cellulose Nanofibril-Based Thin Films To Achieve Highly Fire-Protecting Coatings for Flammable Solid Materials, ACS applied materials & interfaces, 10 (2018) 32543-32555.

[41] S. Zhang, S.-N. Li, Q. Wu, Q. Li, J. Huang, W. Li, W. Zhang, S. Wang, Phosphorus containing group and lignin toward intrinsically flame retardant cellulose nanofibril-based film with enhanced mechanical properties, Composites Part B: Engineering, 212 (2021) 108699.

[42] V. Agarwal, P.B. Zetterlund, Strategies for reduction of graphene oxide – A comprehensive review, Chemical Engineering Journal, 405 (2021) 127018.

[43] M.-Y. Lim, Y.-S. Choi, J. Kim, K. Kim, H. Shin, J.-J. Kim, D.M. Shin, J.-C. Lee, Cross-linked graphene oxide membrane having high ion selectivity and antibacterial activity prepared using tannic acid-functionalized graphene oxide and polyethyleneimine, Journal of Membrane Science, 521 (2017) 1-9.

[44] Y. Lei, Z. Tang, R. Liao, B. Guo, Hydrolysable tannin as environmentally friendly reducer and stabilizer for graphene oxide, Green Chemistry, 13 (2011) 1655–1658.

[45] A. Deniz, N. Zaytoun, L. Hetjens, A. Pich, Polyphosphazene–Tannic Acid Colloids as Building Blocks for Bio-Based Flame-Retardant Coatings, ACS Applied Polymer Materials, 2 (2020) 5345-5351.

[46] Y.-O. Kim, J. Cho, H. Yeo, B.W. Lee, B.J. Moon, Y.-M. Ha, Y.R. Jo, Y.C. Jung, Flame Retardant Epoxy Derived from Tannic Acid as Biobased Hardener, ACS Sustainable Chemistry & Engineering, 7 (2019) 3858-3865.

[47] C.-F. Cao, G.-D. Zhang, L. Zhao, L.-X. Gong, J.-F. Gao, J.-X. Jiang, L.-C. Tang, Y.-W. Mai, Design of mechanically stable, electrically conductive and highly hydrophobic three-dimensional graphene nanoribbon composites by modulating the interconnected network on polymer foam skeleton, Composites Science and Technology, 171 (2019) 162-170.

[48] C.-F. Cao, P.-H. Wang, J.-W. Zhang, K.-Y. Guo, Y. Li, Q.-Q. Xia, G.-D. Zhang, L. Zhao, H. Chen, L. Wang, J.-F. Gao, P. Song, L.-C. Tang, One-step and green synthesis of lightweight, mechanically flexible and flame-retardant polydimethylsiloxane foam nanocomposites via surface-assembling ultralow content of graphene derivative, Chemical Engineering Journal, 393 (2020) 124724.

[49] K.-Y. Guo, Q. Wu, M. Mao, H. Chen, G.-D. Zhang, L. Zhao, J.-F. Gao, P. Song, L.-C. Tang, Water-based hybrid coatings toward mechanically flexible, super-hydrophobic and flame-retardant polyurethane foam nanocomposites with high-efficiency and reliable fire alarm response, Composites Part B: Engineering, 193 (2020) 108017.

[50] N.-J. Huang, C.-F. Cao, Y. Li, L. Zhao, G.-D. Zhang, J.-F. Gao, L.-Z. Guan, J.-X. Jiang, L.-C. Tang, Silane grafted graphene oxide papers for improved flame resistance and fast fire alarm response, Composites Part B: Engineering, 168 (2019) 413-420.

[51] Y. Zhu, S. Murali, W. Cai, X. Li, J.W. Suk, J.R. Potts, R.S. Ruoff, Graphene and graphene oxide: synthesis, properties, and applications, Adv Mater, 22 (2010) 3906-3924.

[52] J. Luo, J. Lai, N. Zhang, Y. Liu, R. Liu, X. Liu, Tannic Acid Induced Self-Assembly of Three-Dimensional Graphene with Good Adsorption and Antibacterial Properties, ACS Sustainable Chemistry & Engineering, 4 (2016) 1404-1413.

[53] F. Luo, K. Wu, J. Shi, X. Du, X. Li, L. Yang, M. Lu, Green reduction of graphene oxide by polydopamine to a construct flexible film: superior flame retardancy and high thermal conductivity, Journal of Materials Chemistry A, 5 (2017) 18542-18550.

[54] S. Song, Y. Zhai, Y. Zhang, Bioinspired Graphene Oxide/Polymer Nanocomposite Paper with High Strength, Toughness, and Dielectric Constant, ACS Appl Mater Interfaces, 8 (2016) 31264-31272.

[55] P. Song, Z. Xu, Y. Wu, Q. Cheng, Q. Guo, H. Wang, Super-tough artificial nacre based on graphene oxide via synergistic interface interactions of π-π stacking and hydrogen bonding, Carbon, 111 (2017) 807-812.

[56] W. Yang, Z. Zhao, K. Wu, R. Huang, T. Liu, H. Jiang, F. Chen, Q. Fu, Ultrathin flexible reduced graphene oxide/cellulose nanofiber composite films with strongly anisotropic thermal conductivity and efficient electromagnetic interference shielding, Journal of Materials Chemistry C, 5 (2017) 3748-3756.

[57] L. Dong, C. Hu, L. Song, X. Huang, N. Chen, L. Qu, A Large-Area, Flexible, and Flame-Retardant Graphene Paper, Advanced Functional Materials, 26 (2016) 1470-1476.

[58] Z.-R. Yu, S.-N. Li, J. Zang, M. Zhang, L.-X. Gong, P. Song, L. Zhao, G.-D. Zhang, L.-C. Tang, Enhanced mechanical property and flame resistance of graphene oxide nanocomposite paper modified with functionalized silica nanoparticles, Composites Part B: Engineering, 177 (2019) 107347.

[59] N.-J. Huang, Q.-Q. Xia, Z.-H. Zhang, L. Zhao, G.-D. Zhang, J.-F. Gao, L.-C. Tang, Simultaneous improvements in fire resistance and alarm response of GO paper via one-step 3-mercaptopropyltrimethoxysilane functionalization for efficient fire safety and prevention, Composites Part A: Applied Science and Manufacturing, 131 (2020) 105797.

[60] P. Ming, Z. Song, S. Gong, Y. Zhang, J. Duan, Q. Zhang, L. Jiang, Q. Cheng, Nacre-inspired integrated nanocomposites with fire retardant properties by graphene oxide and montmorillonite, Journal of Materials Chemistry A, 3 (2015) 21194-21200.

[61] L. Li, X. Liu, X. Shao, L. Jiang, K. Huang, S. Zhao, Synergistic effects of a highly effective intumescent flame retardant based on tannic acid functionalized graphene on the flame retardancy and smoke suppression properties of natural rubber, Composites Part A: Applied Science and Manufacturing, 129 (2020) 105715.

[62] Z.-H. Zhang, J.-W. Zhang, C.-F. Cao, K.-Y. Guo, L. Zhao, G.-D. Zhang, J.-F. Gao, L.-C. Tang, Temperature-responsive resistance sensitivity controlled by L-ascorbic acid and silane co-functionalization in flame-retardant GO network for efficient fire early-warning response, Chemical Engineering Journal, 386 (2020) 123894.

[63] E. Guillaume, V. Dréan, B. Girardin, T. Fateh, Reconstruction of the Grenfell Tower fire – Part 4: Contribution to the understanding of fire propagation and behaviour during horizontal fire spread, Fire and Materials, 44 (2020) 1072-1098.

[64] H. Xu, Y. Li, N.-J. Huang, Z.-R. Yu, P.-H. Wang, Z.-H. Zhang, Q.-Q. Xia, L.-X. Gong, S.-N. Li, L. Zhao, G.-D. Zhang, L.-C. Tang, Temperature-triggered sensitive resistance transition of graphene oxide wide-ribbons wrapped sponge for fire ultrafast detecting and early warning, Journal of Hazardous Materials, 363 (2019) 286-294.

[65] C.-F. Cao, W.-J. Liu, H. Xu, K.-X. Yu, L.-X. Gong, B.-F. Guo, Y.-T. Li, X.-L. Feng, L.-Y. Lv, H.-T. Pan, L. Zhao, J.-Y. Li, J.-F. Gao, G.-D. Zhang, L.-C. Tang, Temperature-induced resistance transition behaviors of melamine sponge composites wrapped with different graphene oxide derivatives, Journal of Materials Science & Technology, 85 (2021) 194-204.

[66] B. Akkaya, B. Çakiroğlu, M. Özacar, Tannic Acid-Reduced Graphene Oxide Deposited with Pt Nanoparticles for Switchable Bioelectronics and Biosensors Based on Direct Electrochemistry, ACS Sustainable Chemistry & Engineering, 6 (2018) 3805-3814.

[67] S. Yoo, X. Li, Y. Wu, W. Liu, X. Wang, W. Yi, Ammonia Gas Detection by Tannic Acid Functionalized and Reduced Graphene Oxide at Room Temperature, Journal of Nanomaterials, 2014 (2014) 1-6.

[68] W. Chen, P. Liu, Y. Liu, Q. Wang, W. Duan, A temperature-induced conductive coating via layer-by-layer assembly of functionalized graphene oxide and carbon nanotubes for a flexible, adjustable response time flame sensor, Chemical Engineering Journal, 353 (2018) 115-125.

[69] J. Wang, J. He, L. Ma, Y. Zhang, L. Shen, S. Xiong, K. Li, M. Qu, Multifunctional conductive cellulose fabric with flexibility, superamphiphobicity and flame-retardancy for all-weather wearable smart electronic textiles and high-temperature warning device, Chemical Engineering Journal, 390 (2020) 124508.

[70] M. Mao, H. Xu, K.-Y. Guo, J.-W. Zhang, Q.-Q. Xia, G.-D. Zhang, L. Zhao, J.-F. Gao, L.-C. Tang, Mechanically flexible, super-hydrophobic and flame-retardant hybrid nano-silica/graphene oxide wide ribbon decorated sponges for efficient oil/water separation and fire warning response, Composites Part A: Applied Science and Manufacturing, 140 (2021) 106191.

[71] Z. Zhang, D. Yang, H. Yang, Y. Li, S. Lu, R. Cai, W. Tan, A Hydrophobic Sisal Cellulose Microcrystal Film for Fire Alarm Sensors, Nano letters, 21 (2021) 2104-2110.

[72] Q. Liu, S. Yang, J. Ren, S. Ling, Flame-Retardant and Sustainable Silk Ionotronic Skin for Fire Alarm Systems, ACS Materials Letters, 2 (2020) 712-720.

[73] Z.-R. Yu, M. Mao, S.-N. Li, Q.-Q. Xia, C.-F. Cao, L. Zhao, G.-D. Zhang, Z.-J. Zheng, J.-F. Gao, L.-C. Tang, Facile and green synthesis of mechanically flexible and flame-retardant clay/graphene oxide nanoribbon interconnected networks for fire safety and prevention, Chemical Engineering Journal, 405 (2021) 126620.

[74] R.J. Smith, K.M. Holder, S. Ruiz, W. Hahn, Y. Song, Y.M. Lvov, J.C. Grunlan, Environmentally Benign Halloysite Nanotube Multilayer Assembly Significantly Reduces Polyurethane Flammability, Advanced Functional Materials, 28 (2017) 1703289.

[75] Y.S. Kim, Y.-C. Li, W.M. Pitts, M. Werrel, R.D. Davis, Rapid Growing Clay Coatings to Reduce the Fire Threat of Furniture, ACS applied materials & interfaces, 6 (2014) 2146-2152.

Declaration of interests

☒ The authors declare that they have no known competing financial interests or personal relationships that could have appeared to influence the work reported in this paper.

☐The authors declare the following financial interests/personal relationships which may be considered as potential competing interests:

Figures and Table captions

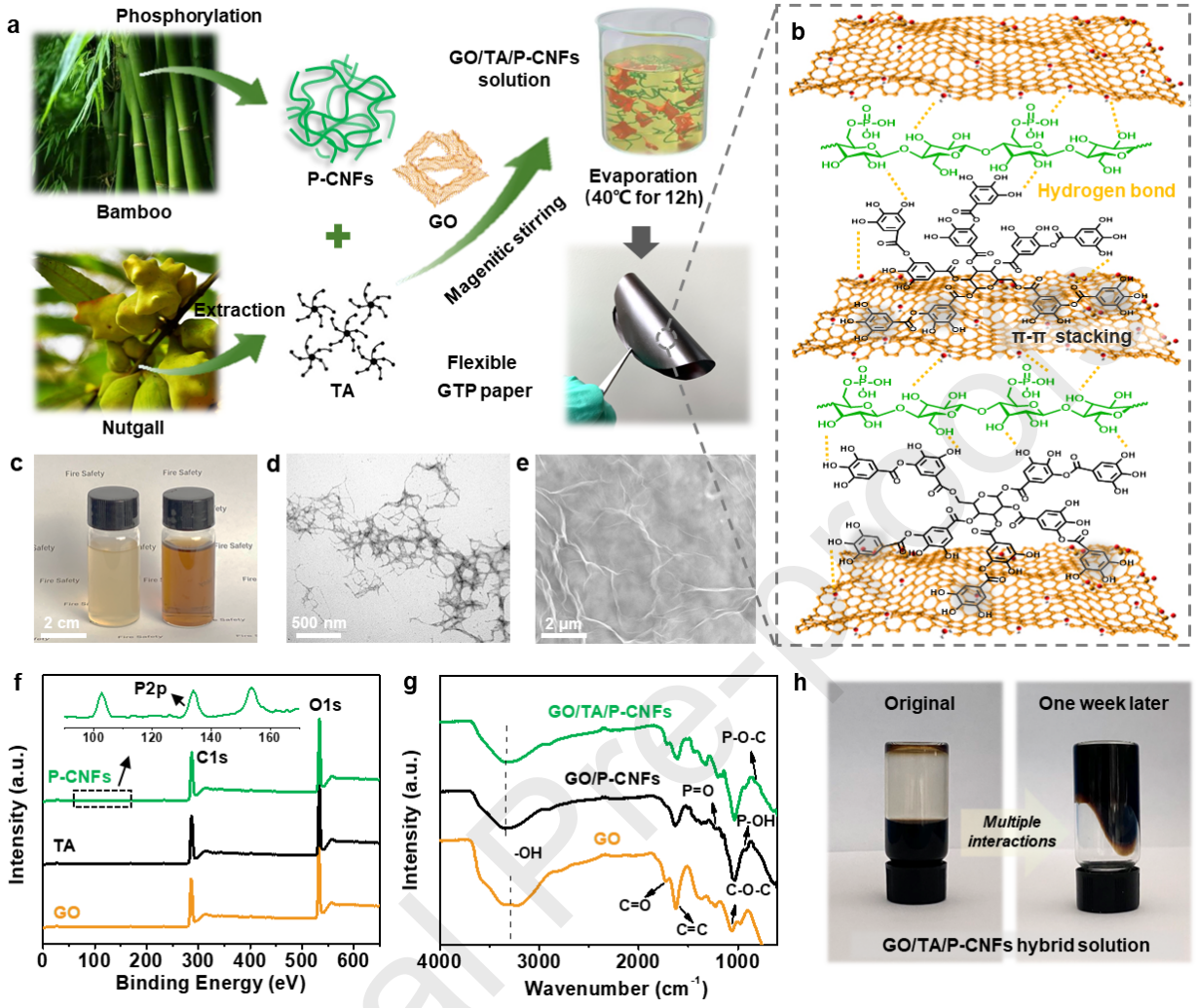

Figure 1. Fabricating process and characterizations. (a) Scheme for preparing the GTP paper nanocomposites via evaporation-induced self-assembly strategy, and (b) schematic of multiple interactions between GO, TA, and P-CNFs; (c) Digital photographs of P-CNFs (left) and GO (right) water solution; (d) TEM image of P-CNFs and (e) SEM image of GO sheets; (f) XPS survey of GO, TA, and P-CNFs; (g) FTIR spectra of GO, GO/P-CNFs and GO/TA/P-CNFs nanocomposites papers; (h) Images of GO/TA/P-CNFs solution: original (left) and (right) stand for one week. The increase of viscosity of hybrid solution further

indicates multiple interactions between GO, TA, and P-CNFs.

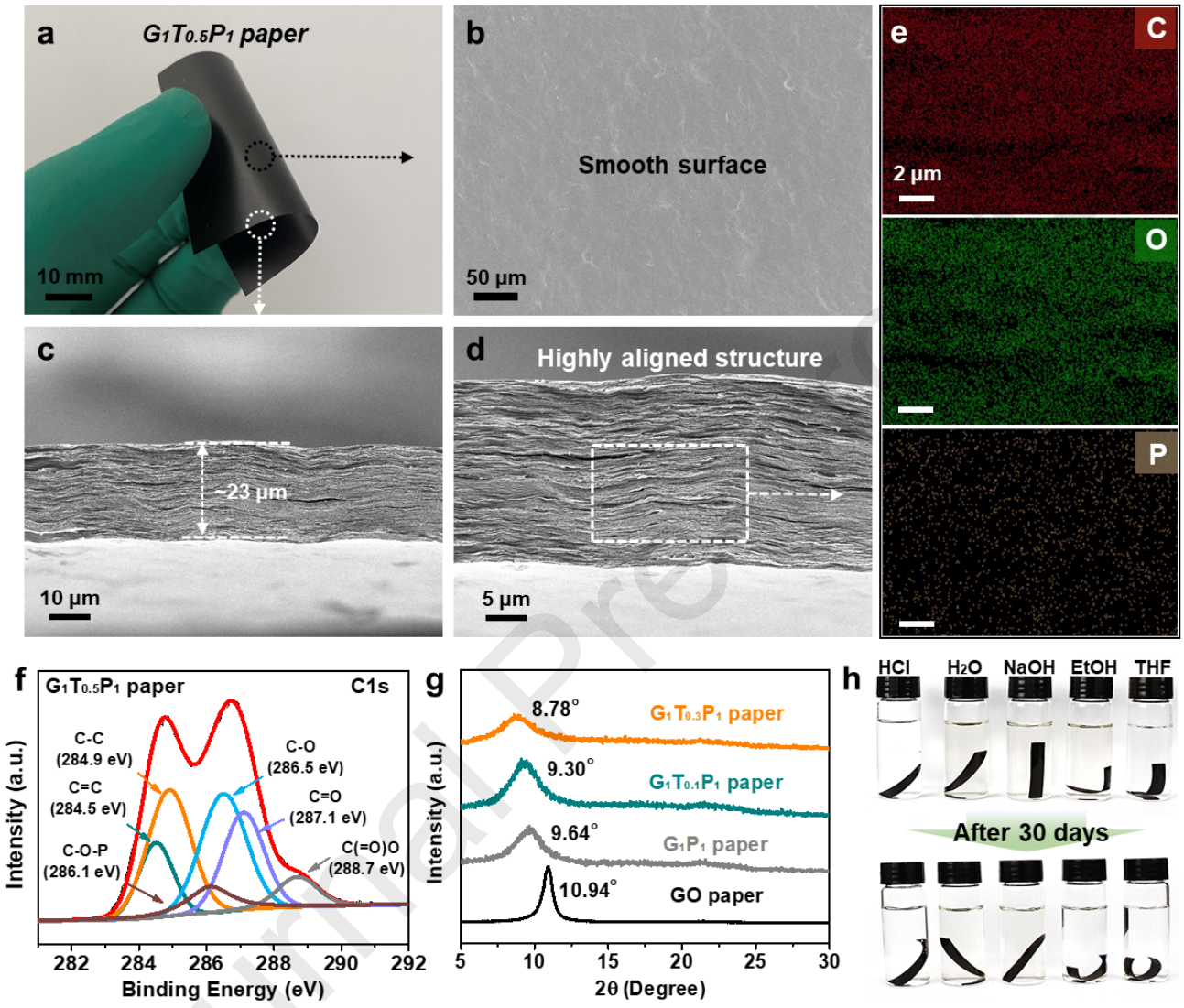

Figure 2. Structural characterization and analysis of GTP paper. (a) Digital photograph of $G_1T_{0.5}P_1$ paper, showing good mechanical flexibility. (b) Typical surface and (c,d) cross-sectional SEM images of $G_1T_{0.5}P_1$ paper and its (e) EDS mapping images for C, O and P, respectively. (f) C1s XPS spectra of $G_1T_{0.5}P_1$ paper and (g) XRD patterns of GTP paper samples. (h) Structure stability of $G_1T_{0.5}P_1$ paper before and after being

immersed in various solutions for one month, including HCl, H_2O, NaOH, EtOH and THF.

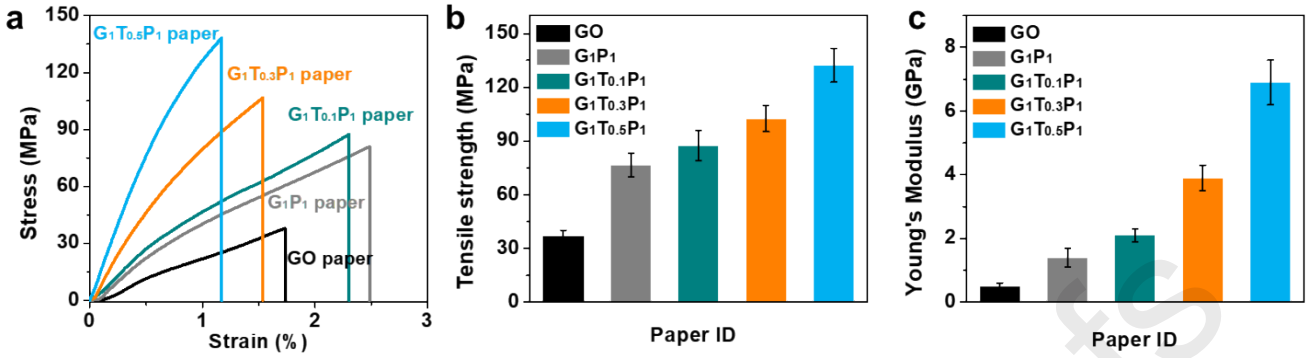

Figure 3. (a) Tensile stress-strain curves, (b) tensile strength and (c) Young's modulus of various composite papers, confirming the synergistic reinforcing effect between the GO, TA, and P-CNFs.

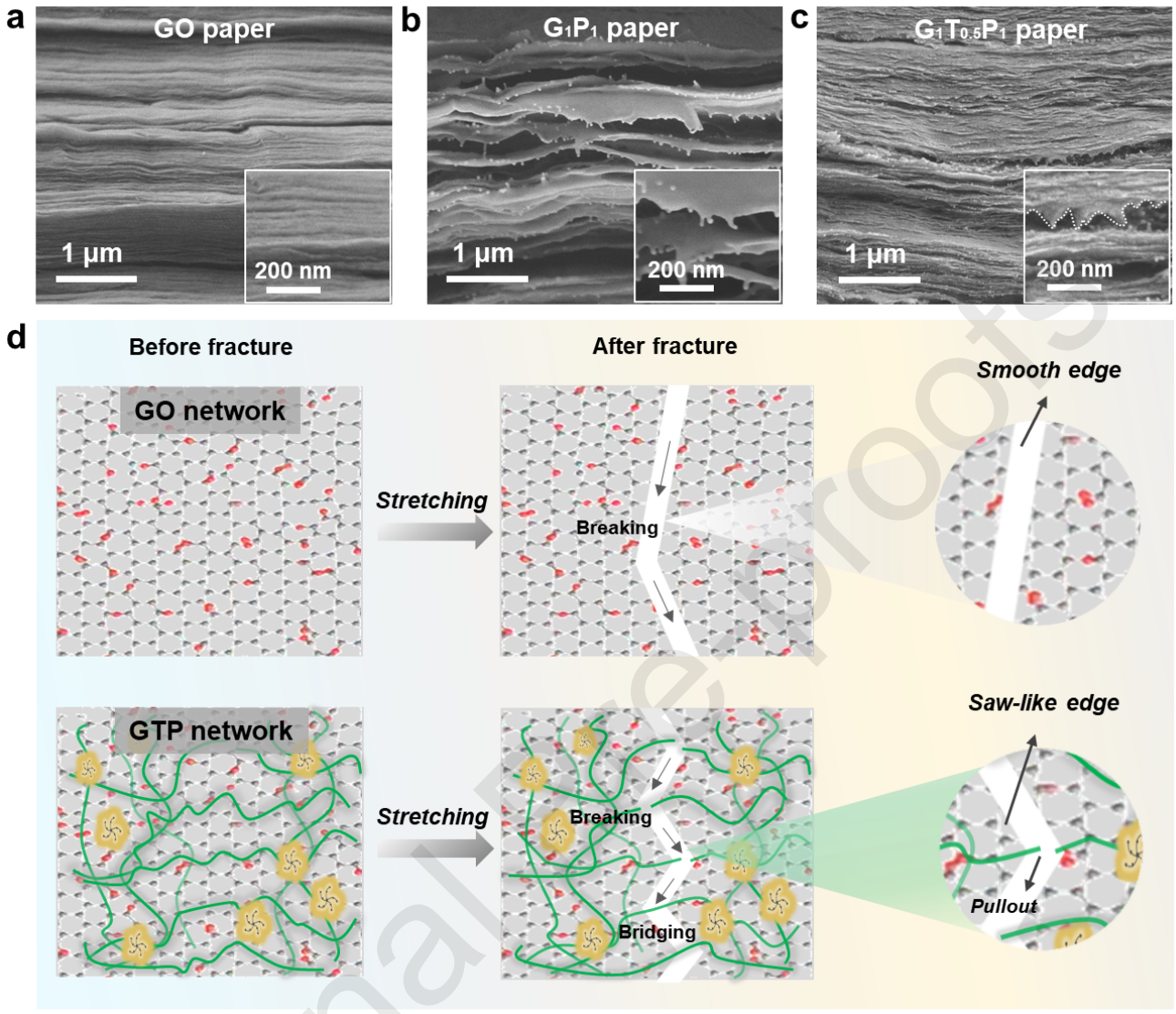

Figure 4. The SEM images of cross-section morphology: (a) GO paper, (b) G_1P_1 paper, (c) $G_1T_{0.5}P_1$ paper, respectively. (d) Proposed synergistic reinforcing mechanism of GO/TA/P-CNFs ternary paper nanocomposites. When stretching starts, the GO nanosheets begin to slide and initiate the crack. With continuous stretching, the P-CNFs bridge the crack and restrict GO nanosheet further continuous sliding. Besides, due to the presence of TA molecules, the crosslinked sites in GO/TA/P-CNFs hybrid network via

multiple interfacial interactions i.e., hydrogen bonding and π-π stacking. Finally, the ternary GTP paper nanocomposites fracture in the mode of P-CNFs pullout.

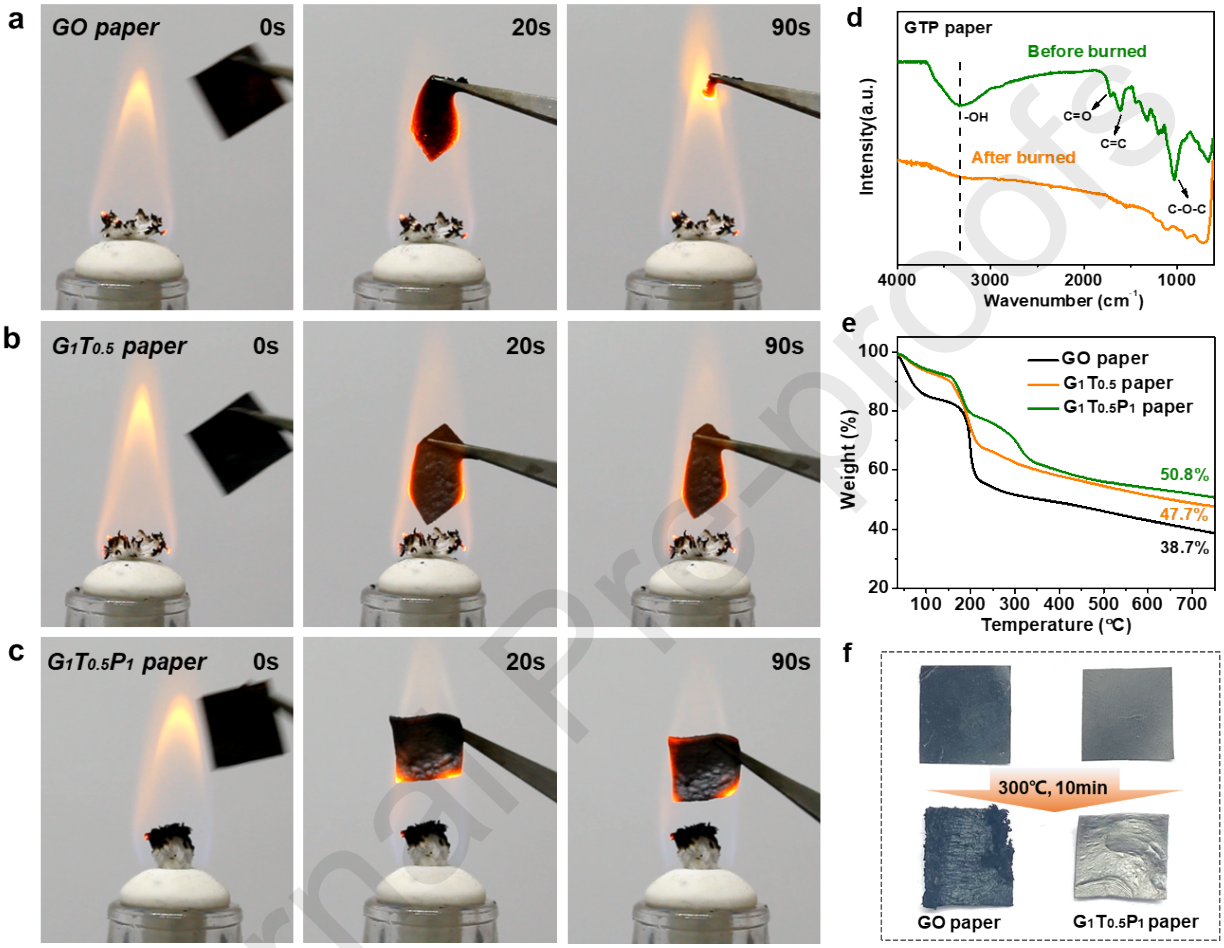

Figure 5. Flame-retardant performance and thermal stability of various paper nanocomposites. The combustion process of (a) GO, (b) $G_1T_{0.5}$ and (c) $G_1T_{0.5}P_1$ papers, respectively, showing improved flame resistance with the presence of TA and P-CNFs. (d) FTIR spectra of GTP paper before /after burned. (e) TGA results of various paper samples. (f) Digital photographs of GO paper and GTP paper before and after 300 °C for 10 min, indicating that the introduction of TA and P-CNFs can improve structural integrity of paper

nanocomposites effectively under high-temperature condition.

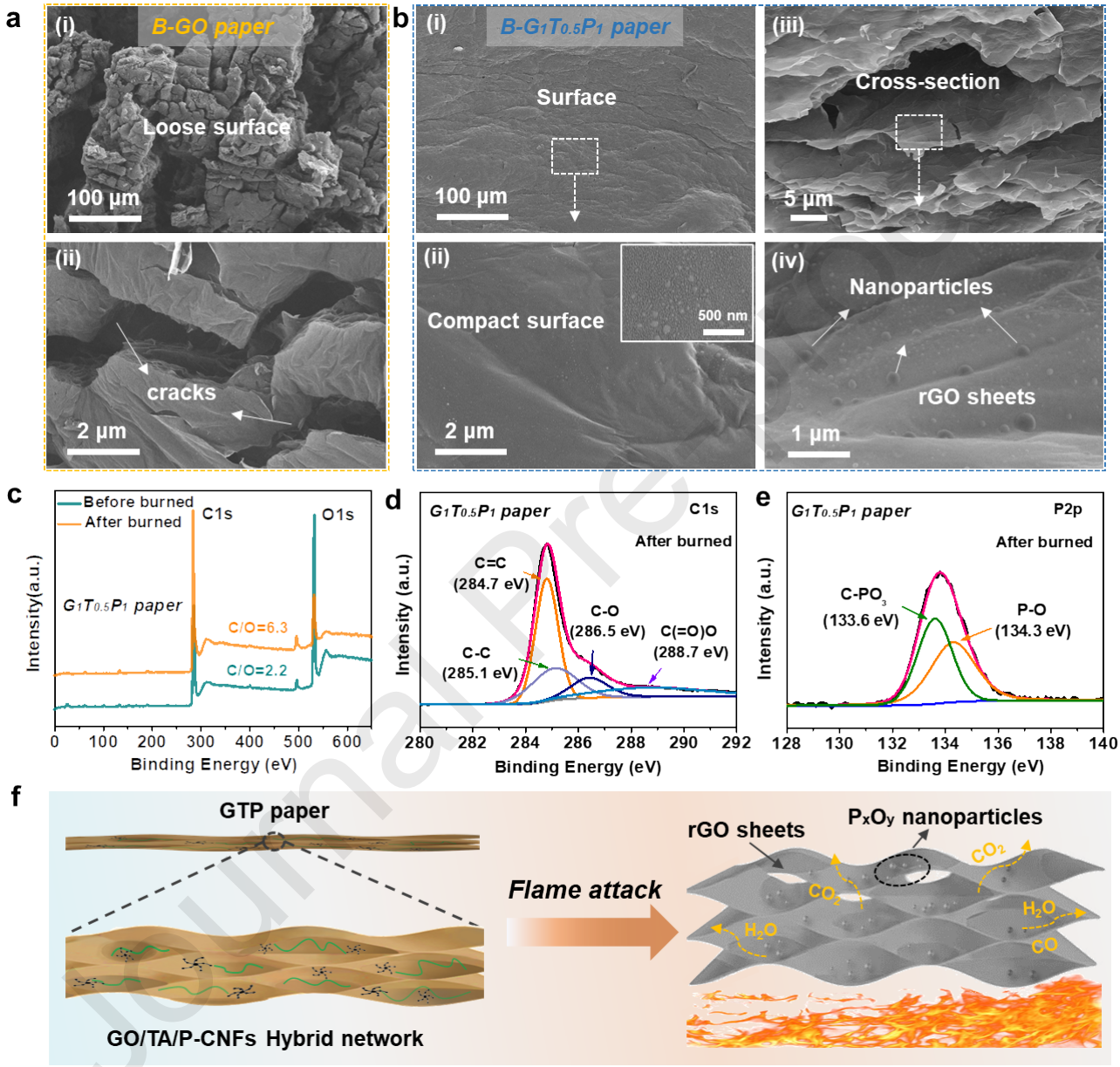

Figure 6. Flame-retardant mechanism analysis. Surface and cross-section SEM images of (a) GO paper and (b) $G_1T_{0.5}P_1$ paper after burned. (c) XPS spectra of $G_1T_{0.5}P_1$ paper before and after burned; (d) C1s and (e) P2p XPS spectrum of $G_1T_{0.5}P_1$ paper after burned. (f) Schematic illustration of the proposed flame-retardant

mechanism of GTP paper under flame attack.

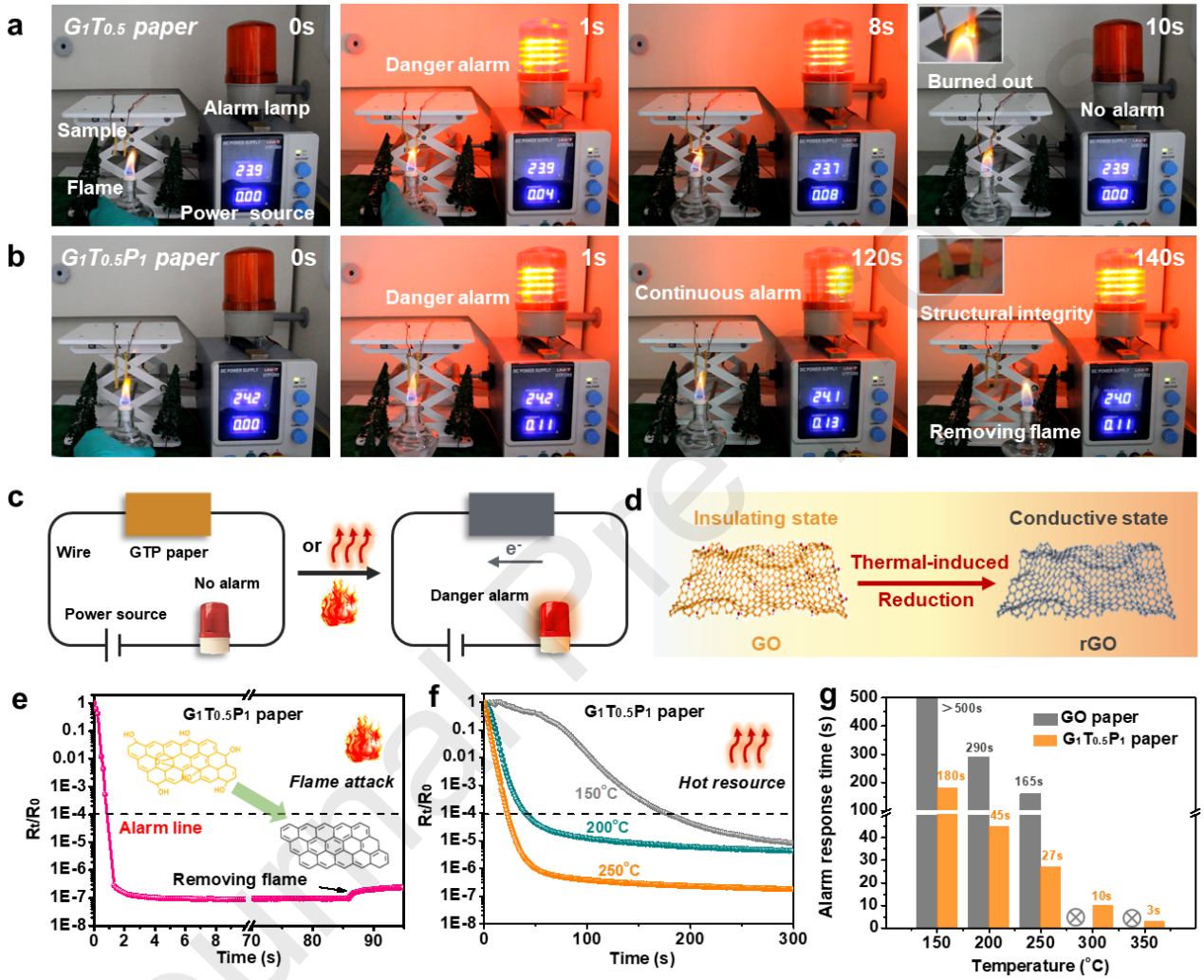

Figure 7. Flame rapid detection and early warning behaviors. Photographs of flame detection processes of (a) $G_1T_{0.5}$ and (b) $G_1T_{0.5}P_1$ papers; (c) schematic illustration of fire alarm sensor based on GTP paper under flame attack and (d) its corresponding resistance transition (from insulating to conductive state) due to thermal-induced reduction of GO. Electrical resistance changes of the GTP network under (e) flame attack

and (f) different environmental temperatures, showing rapid fire early warning alarm response below the ignition temperature of most combustible materials. (g) Alarm responsive time of GO and $G_1T_{0.5}P_1$ papers under different high-temperature conditions from 150 to 350 °C.

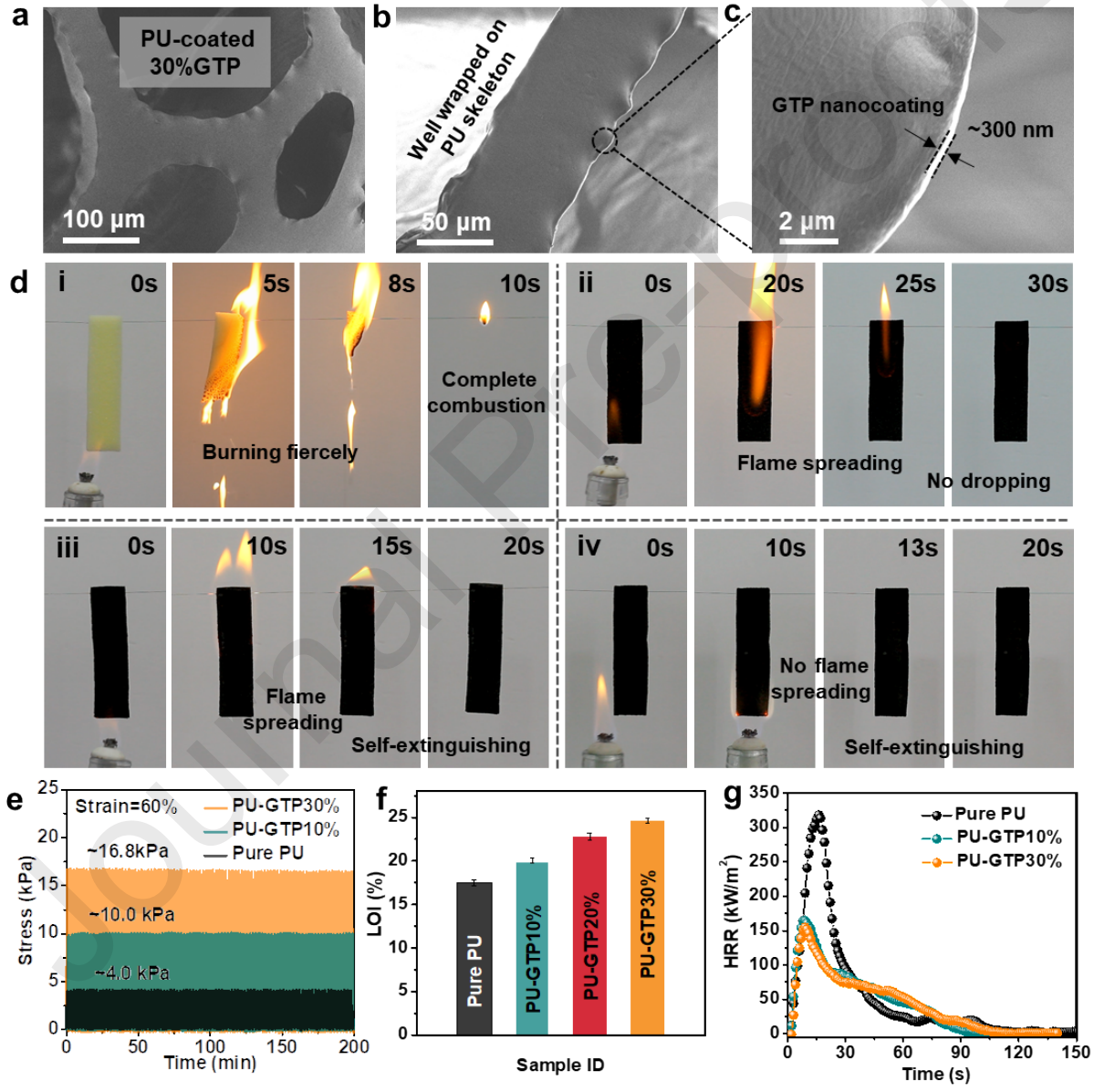

Figure 8. (a-c) SEM images of PU coated with GTP nanocoating; (d) Fire ignition behavior for various PU

composites: (i) pure PU foam, (ii) PU-GTP10%, (iii) PU-GTP20% and (iv) PU-GTP30%. (e) Typical cyclic compressive tests of samples, showing excellent mechanical flexibility and structural reliability. (f) Limited oxygen index (LOI) values and (g) Heat release rate curves of various PU foam materials.

Table 1. Comparison of the early fire warning sensor based on GO/TA/P-CNFs with other previously reported fire alarm systems.

Composition and type of composite materials [a]	Fabrication method	Sustainability	Flame alarm time (s)	High temperature warning time (s)	R
GO/silicone coating	Dip coating in alcohol and water solution	No	<3	13 s at 350 °C; 38 s at 300 °C 87 s at 250 °C; 415 s at 200 °C	[2
FGO/CNTs coated WPP	LbL in ethanol and acetic acid	No	~5	18 s at 400 °C	[6
Silane-GO paper	Gel assembly in water solution	No	~1.6	NM	[3
MF@GOWR sponge	Dip coating in water solution	No	2.1	2.9 s at 450 °C; 5.7 s at 400 °C 33.5 s at 300 °C; 334.2 s at 200 °C	[6
MWCNT nanofluid coated CF	Spray-coating with ethanol	No	21	NM	[3
RGOP-NaCl strip	EISA in water solution	No	~5.3	NM	[2
MPTS-GO paper	EISA in water solution	No	~1	8 s at 400 °C; 35 s at 300 °C 86 s at 250 °C; 232 s at 200 °C	[3
I/MSF-g-COOH/CA/GN film	EISA in water solution	Yes	~1	NM	[1
GO/PDMAEMA/BN coated CF	Dip coating in water and UV irradiation	No	<3	15 s at 219 °C	[2
GONR/MMT/PEG paper	Dip coating in water solution	No	~2	11 s at 400 °C; 79 s at 300 °C 160 s at 250 °C; 450 s at 200 °C	[1
Ag/PANI coated CF	Dip coating in ethanol and water solution	No	<3	>40 s at <300 °C; <3 s at >400 °C	[6
SF/Ca^{2+} i-skin	Dialysis and film casting with formic acid solution	Yes	<50	NM	[1
GO/BP-MoS_2 film	Vacuum filtration in water solution	No	~1	44 s at 300 °C; 130 s at 150 °C	[2
GOWR/silane hybrid coated MF sponge	Dip coating in water solution and THF	No	~3	12 s at 350 °C; 39 s at 300 °C 158 s at 250 °C; 658 s at 200 °C	[1
GO/TA/P-CNFs paper	*EISA in water solution*	*Yes*	*<1*	*3 s at 350 °C; 10 s at 300 °C* *27 s at 250 °C; 45 s at 200 °C* *180 s at 150 °C*	*T w*

[a] Notes: GO: graphene oxide; F-GO: functionalized GO; CNTs: carbon nanotubes; WPP: wood pulp paper;

MF: melamine foam; GOWR : graphene oxide wide ribbon; MWCNT: multi-wall carbon nanotube; CF: cotton fabric; RGOP: reduced graphene oxide paper; MPTS: 3-mercaptopropyltrimethoxysilane; SPI: soy protein isolate; MSF-g-COOH: sisal cellulose microcrystals; CA: citric acid; GN: graphene nanosheets; PDMAEMA: polydimethylaminoethylmethacrylate; BN: boron nitrid; GONR: graphene oxide narrow ribbon; MMT: montmorillonite; PEG: polyethylene glycol; PANI: polyaniline; SF: silk fibroin; BP: black phosphorus; MoS_2: molybdenum disulfide; TA: tannic acid; P-CNFs: phosphorylated cellulose nanofibrils; LbL: Layer by Layer; EISA: evaporation-induced self-assembly.

[b] NM: not mentioned.

Graphical Abstract

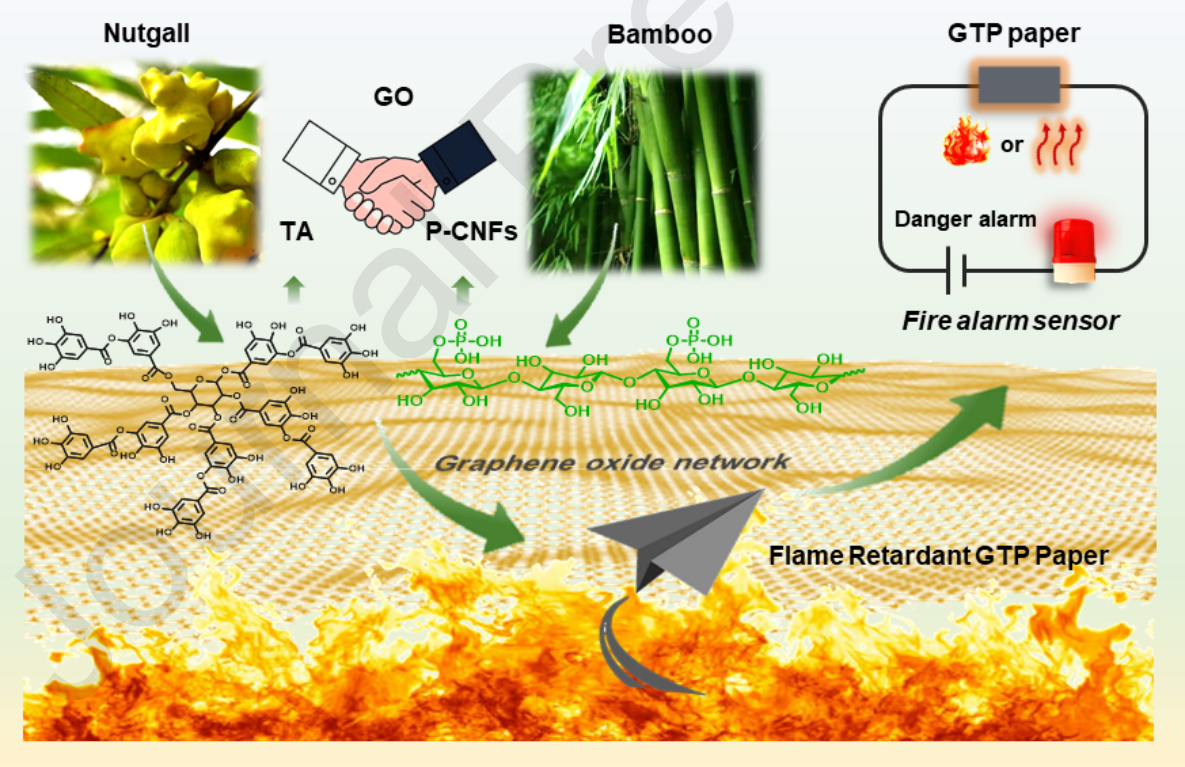

Two natural biomass derivatives i.e., tannic acid (TA) and phosphorylated-cellulose nanofibrils (P-CNFs) were employed to decorate graphene oxide network and the as-prepared flame-retardant GTP paper with

ultrasensitive fire alarm response can be applied as desirable smart fire alarm sensor material.

Highlights

- Biomass-derivatives decorated graphene oxide network was fabricated via a facile strategy.
- The synergistic reinforcing effect was formed in the hybrid networks based on bionic design.
- The bio-based hybrid networks show excellent flame resistance and structural stability.
- Ultrasensitive fire alarm time of <1s and desirable fire early warning responses are achieved.
- Such hybrid networks can be used as sustainable fireproof and fire alarm sensor materials.